Available online at www.sciencedirect.com
SCIENCE DIRECT®
Icarus 169 (2004) 216–241
ICARUS
www.elsevier.com/locate/icarus

A thermodynamic model of high temperature lava vaporization on Io

Laura Schaefer and Bruce Fegley Jr. *

Planetary Chemistry Laboratory, Department of Earth and Planetary Sciences, Washington University, One Brookings Dr., Campus Box 1169, St. Louis, MO 63130, USA

Received 1 April 2003; revised 23 July 2003

Abstract

We modified the MAGMA chemical equilibrium code developed by Fegley and Cameron (1987, Earth Planet. Sci. Lett. 82, 207–222) and used it to model vaporization of high temperature silicate lavas on Io. The MAGMA code computes chemical equilibria in a melt, between melt and its equilibrium vapor, and in the gas phase. The good agreement of MAGMA code results with experimental data and with other computer codes is demonstrated. The temperature-dependent pressure and composition of vapor in equilibrium with lava is calculated from 1700 to 2400 K for 109 different silicate lavas in the O–Na–K–Fe–Si–Mg–Ca–Al–Ti system. Results for five lavas (tholeiitic basalt, alkali basalt, Barberton komatiite, dunite, and a molten type B1 Ca, Al-rich inclusion) are discussed in detail. The effects of continuous fractional vaporization on chemistry of these lavas and their equilibrium vapor are presented. The predicted abundances (relative to Na) of K, Fe, Si, Al, Ca, and Ti in the vapor equilibrated with lavas at 1900 K are lower than published upper limits for Io's atmosphere (which do not include Mg). We predict evaporative loss of alkalis, Fe, and Si during volcanic eruptions. Sodium is more volatile than K, and the Na/K ratio in the gas is decreased by fractional vaporization. This process can match Io's atmospheric Na/K ratio of 10 ± 3 reported by Brown (2001, Icarus 151, 190–195). Silicon monoxide is an abundant species in the vapor above lavas. Spectroscopic searches are recommended for SiO at IR and mm wavelengths. Reactions of metallic vapors with S- and Cl-bearing volcanic gases may form other unusual gases including $MgCl_2$, MgS, MgCl, $FeCl_2$, FeS, FeCl, and SiS.

Keywords: Io; Volcanism; Geochemistry; Lava; Magma; Vaporization; Vapor pressure; High temperature; Alkalis; Sodium; Potassium; Silicon; Iron; Magnesium; Calcium; Aluminum; Titanium; Silicon monoxide; Basalt; Komatiite; Dunite; Tholeiite; CAI

1. Introduction

Voyagers 1 and 2 discovered active volcanism on Io (Morabito et al., 1979; Smith et al., 1979b). Subsequent Earth-based observations showed that Io is the most volcanically active body in our Solar System, with a heat flux more than 20 times greater than the Earth (Spencer and Schneider, 1996). Voyagers 1 and 2 observed temperatures of 300–650 K on Io. At that time S and O were the only elements observed in Io's atmosphere. Thus, Sagan (1979) and Smith et al. (1979a) suggested sulfur and/or SO_2 volcanism on Io. However, the Voyager IR spectrometers could not detect temperatures > 650 K (Pearl and Sinton, 1982).

Ground-based and HST observations between 1980 and 1995 detected several high temperature out-bursts with temperatures more in keeping with silicate volcanism (Veeder et al., 1994; Carr, 1986; Spencer and Schneider, 1996). More recently, the Galileo mission provided further evidence of high temperature silicate volcanism. Two hot spots with very high observed temperatures are Pele and Pillan (Lopes et al., 2001; Davies et al., 2001; Radebaugh et al., this issue). Pele is described as a lava lake with fairly consistent temperatures around 1300–1400 K, with periodic brightenings indicating temperatures of 1760 ± 210 K (Lopes et al., 2001; Radebaugh et al., this issue). Pillan does not have temperatures as consistently high as Pele but has produced the highest temperature so far observed (1870 K) during a several months long eruption that produced a ring of pyroclastic deposits 400 km in diameter (Davies et al., 2001).

Significant vapor pressures of alkalis and other elements exist above solid and liquid oxides and silicates at the observed hot spot temperatures. These vapor pressures exceed Io's atmospheric pressure of $\sim$ 1–10 nanobars by orders of magnitude. A few examples should suffice to illustrate this point.

Mass spectrometric studies of the vapor produced by heating pieces of the Holbrook L6 chondrite to 1573 K

* Corresponding author.
E-mail address: bfegley@levee.wustl.edu (B. Fegley).

0019-1035/$ – see front matter
doi:10.1016/j.icarus.2003.08.023

showed maximum vapor pressures of $10^{-5.3\pm0.3}$ bars for Na, $10^{-5.8\pm0.3}$ bars for K, and $10^{-5.3\pm0.3}$ bars for Fe gases (Gooding and Muenow, 1977). DeMaria et al. (1971), Naughton et al. (1971), and Markova et al. (1986) did mass spectrometric studies of the vapor evolved from lunar basalts heated up to and above their liquidus temperatures ($\sim$ 1423 K). DeMaria et al. (1971) observed sequential vaporization of Na, K, Fe, Mg, Si (as SiO and SiO_2), Ca, Al (as Al, Al_2O, and AlO), and Ti (as TiO and TiO_2) as an Apollo 12 basalt (#12002) was heated up to 2500 K. Partial vapor pressures of Na, Fe, Mg, SiO, Ca, Al, and TiO reached 10^{-6} bars at temperatures of about 1430, 1600, 1720, 1800, 2040, 2070, and 2190 K, respectively. Naughton et al. (1971) observed vaporization of a number of Na and K gases (Na, Na_2, NaO, K, KO, K_2O, K_2) with maximum pressures of $\sim 10^{-7}$ bars for Na and K as the same basalt was heated up to 1400 K. Markova et al. (1986) heated an Apollo 16 basalt (#68415) up to 2500 K, observed sequential vaporization of Na, K, Fe, Si, Mg, Ca, Ti, and Al, identified the major vapor species of each element, and generally made observations similar to those of DeMaria et al. (1971).

A large number of mass spectrometric studies have been done on the vapor composition and pressure above solid and liquid silica in the temperature range 1800–2200 K (e.g., Porter et al., 1955; Nagai et al., 1973; Zmbov et al., 1973; Shornikov et al., 1998, and references therein). These studies show that SiO, SiO_2, O_2, and O are the major vapor species, with SiO being more abundant than SiO_2. Partial vapor pressures of SiO typically vary from $\sim 7 \times 10^{-6}$ bars at 1800 K to $\sim 5 \times 10^{-5}$ bars at 2100 K. All these experiments as well as others summarized by Stolyarova and Semenov (1994) and Stolyarova (2001) indicate that rock-forming elements are vaporizing from hot lavas on Io and have significant vapor pressures above these lavas.

We therefore decided to model the vapor pressure and composition above lavas on Io as a function of the type of lava and its temperature. We chose to use the MAGMA computer code, which was developed by Fegley and Cameron (1987) to model vaporization of the planet Mercury during its formation. We started out with several questions in mind:

(1) Is the total pressure or composition of a vapor coexisting in equilibrium with a lava diagnostic of the lava composition?
(2) What vapor species should be searched for above active volcanic vents on Io, and can these species help constrain lava compositions?
(3) How does fractional vaporization, i.e., the continuous loss of all vapor as it is evolved, change lava compositions?

This paper is organized as follows. We first review the algorithm and data used in the MAGMA code. We then present a comparison of MAGMA results with experimental data and results of other computer codes. Following this we describe our choices for lavas to model and the temperature range to use. We then discuss our results, beginning with vapor pressures and vapor compositions. The effects of fractional vaporization on composition of lava and coexisting vapor are also discussed. We finally discuss applications of our results to Io and recommend searching for several vapor species above high temperature hot spots. Preliminary results of our work, done before modifications were made to the MAGMA code, were given by Schaefer and Fegley (2002) and Fegley et al. (2003). Additional discussion of the fractional vaporization calculations, including implications for ceramic volcanism on Io is given by Kargel and Fegley (2002) and Kargel et al. (2003a, 2003b).

2. Computational methods

2.1. Overview

We calculated melt–vapor equilibrium using a modified version of the MAGMA code described by Fegley and Cameron (1987). The MAGMA code is a robust and rapid mass-balance, mass action algorithm which uses the ideal mixing of complex components (IMCC) model developed by Hastie and colleagues at the US National Bureau of Standards (now called NIST) in the 1980s (Hastie et al., 1982a, 1982b; 1984; Hastie and Bonnell, 1985, 1986). The MAGMA code simultaneously solves for:

(1) activity coefficients of metal oxides in non-ideal silicate and oxide melts,
(2) melt–vapor equilibrium, and
(3) vapor equilibrium.

The code considers two cases: melt–vapor equilibrium with and without fractional vaporization. Below, we give a brief description of the code. For a more detailed explanation see Fegley and Cameron (1987).

2.2. Model

The current version of the MAGMA code considers the chemical equilibria of eight metal oxides: MgO, SiO_2, Al_2O_3, TiO_2, FeO, CaO, Na_2O, and K_2O in melts. Chemical equilibria in the melts are modeled using thermodynamic activities (a_i), which are given by

$$a_i = \gamma_i x_i, \tag{1}$$

where x_i is the mole fraction of oxide i in the melt, and γ_i is the Raoultian activity coefficient of oxide i relative to the pure liquid oxide. For an ideal solution, $\gamma_i = 1$, and $a_i = x_i$, i.e., the activity is the same as the mole fraction. For a non-ideal solution, γ_i can have any value greater than zero. The activities of oxides in non-ideal melts are calculated from the mole fractions of unbound oxides in the melt:

$$a_{\text{oxide}} = x^*_{\text{oxide}}, \tag{2}$$

Table 1
Species included in MAGMA code calculations

Melt species	Vapor species
SiO_2,MgO, FeO, CaO, Al_2O_3, TiO_2,	O, O_2
Na_2O, K_2O	Si, SiO, SiO_2
$MgSiO_3$, Mg_2SiO_4, $MgAl_2O_4$,$MgTiO_3$, $MgTi_2O_5$,	Mg, MgO
Mg_2TiO_4,$Mg_2Al_4Si_5O_{18}$	Fe, FeO
$FeTiO_3$, Fe_2SiO_4, $FeAl_2O_4$	Ca, CaO
$CaAl_2O_4$, $CaAl_4O_7$, $Ca_{12}Al_{14}O_{33}$, $CaMgSi_2O_6$,	Al, AlO, AlO_2,
$Ca_2MgSi_2O_7$, $Ca_2Al_2SiO_7$, $CaAl_2Si_2O_8$, $CaTiO_3$,	Al_2O, Al_2O_2
Ca_2SiO_4, $CaTiSiO_5$, $CaAl_{12}O_{19}$, $CaSiO_3$	Ti, TiO, TiO_2
$Al_6Si_2O_{13}$	Na, Na_2, NaO,
Na_2SiO_3, $Na_2Si_2O_5$, $NaAlSiO_4$, $NaAlSi_3O_8$,	Na_2O, Na^+
$NaAlO_2$,Na_2TiO_3, $NaAlSi_2O_6$	K, K_2, KO,
K_2SiO_3, $K_2Si_2O_5$, $K_2Si_4O_9$, $KAlSiO_4$,	K_2O, K^+
$KAlSi_3O_8$,$KAlO_2$, $KAlSi_2O_6$, $KCaAlSi_2O_7$	e^-

where x_i^* is the mole fraction of the unbound oxide in the melt. By definition, $x^*_{\text{oxide}} \leqslant x_{\text{oxide}}$ in the IMCC model because formation of more complex pseudospecies (see Table 1) can reduce the number of unbound oxide molecules. The activity coefficient is calculated from

$$\gamma_i = x_i^*/x_i \tag{3}$$

where x_i is the total mole fraction of the oxide.

For example, the concentrations of MgO and SiO_2 in the melt can be reduced by a reaction such as

$$\text{MgO (liq)} + \text{SiO}_2\text{ (liq)} = \text{MgSiO}_3\text{ (liq)}, \tag{4}$$

which has an equilibrium constant K_4 given by

$$K_4 = \frac{a_{\text{MgSiO}_3}}{a_{\text{MgO}} \times a_{\text{SiO}_2}} \tag{5}$$

and by the reaction

$$2\text{MgO (liq)} + \text{SiO}_2\text{ (liq)} = \text{Mg}_2\text{SiO}_4\text{ (liq)} \tag{6}$$

with an equilibrium constant

$$K_6 = \frac{a_{\text{Mg}_2\text{SiO}_4}}{a^2_{\text{MgO}} \times a_{\text{SiO}_2}}. \tag{7}$$

The activity coefficient for MgO in this system is given by

$$\gamma_{\text{MgO}} = \frac{a_{\text{MgO}}}{a_{\text{MgO}} + a_{\text{MgSiO}_3} + 2 \times a_{\text{Mg}_2\text{SiO}_4}}. \tag{8}$$

The activity of MgO could be reduced by reactions in other binary and ternary systems (e.g., MgO–Al_2O_3–SiO_2). The actual expression for the MgO activity used in the MAGMA code has 10 terms in the denominator. A total of 38 melt species are considered in the MAGMA code (Table 1). The potassium pseudospecies $K_2Si_4O_9$ and $KCaAlSi_2O_7$ are new additions to the code. Thermodynamic data for these new species and revised data for the potassium silicate pseudospecies are given in Table 2, while data for the remaining pseudospecies are given in Table 3 of Fegley and Cameron (1987).

Equilibrium in the melt and between melt and vapor are calculated simultaneously. The melt–vapor equilibria are calculated assuming that the oxides vaporize stoichiometrically, i.e., an SiO_2 molecule vaporizes to gas with a bulk Si/O ratio of 1 : 2. In order to satisfy the dual constraints of mass balance and mass action, the activities of the melt components calculated from the melt–vapor equilibria must equal the activities calculated from the melt chemistry described above. For example, the activity of MgO calculated from the reactions above and from the reaction

$$\text{MgO (liq)} = \text{Mg (g)} + \text{O (g)}, \tag{9}$$

$$K_9 = \frac{P_{\text{Mg}} P_{\text{O}}}{a_{\text{MgO}}} \tag{10}$$

must be equal. The MAGMA code also calculates the equilibrium distribution of the vaporized metals into different gaseous species. A total of 30 gases are considered (Table 1). Thermal ionization products (Na^+, K^+, e^-) are new additions to the code. The thermodynamic data for these species come from the JANAF Tables (Chase, 1998). Thermodynamic data for all other species are the same as given in Tables 1 and 2 of Fegley and Cameron (1987).

Fractional vaporization of the lava, in which mass is continually lost from the system, is computed in a step-wise fashion. As in Fegley and Cameron (1987), the step size is defined by removing 5% of the most volatile metal oxide. Relative proportions of the other metal oxides are also removed. Equilibrium between the vapor and lava is then recomputed. This is repeated until the system has almost completely vaporized. Although the 5% step size is arbitrary, there is no change in the calculated results for step sizes of 1, 2, 4, and 10%.

2.3. Comparisons with prior work

The results from the MAGMA code have been compared to theoretical and experimental work found in the literature.

Table 2
Revised thermodynamic data ($\log_{10} K = A + B/T$)

Reaction	A	B	Ref.
K_2O (liq) + SiO_2 (liq) = K_2SiO_3 (liq)	0.27	12735	Hastie and Bonnell (1985)
K_2O (liq) + $2SiO_2$ (liq) = $K_2Si_2O_5$ (liq)	0.35	14685	Hastie and Bonnell (1985)
K_2O (liq) + $4SiO_2$ (liq) = $K_2Si_4O_9$ (liq)	−0.96	17572	Hastie and Bonnell (1985)
$0.5K_2O$ (liq) + CaO (liq) + $0.5Al_2O_3$ + $2SiO_2$ (liq) = $KCaAlSi_2O_7$ (liq)	4.30	17037	Hastie and Bonnell (1985)
Na (g) = Na^+ (g) + e^- (g)	−15.33	36735	Chase (1998)
K (g) = K^+ (g) + e^- (g)	2.76	23760	Chase (1998)

In principle, it should be possible to compare activity coefficients in melts, the total vapor pressure over melts, the partial vapor pressures of individual gases over melts, and changes in the melt and vapor composition as a function of the amount of melt vaporized. These different comparisons are important because different experimental techniques, which have different errors, are used to obtain these data. In practice, only a few of these comparisons are possible because no experimental data exist or experiments were done using continuous heating instead of isothermal vaporization. Nevertheless, a number of comparisons have been made and are described next. To our knowledge, no other vaporization code has been validated as extensively, and with such good agreement, as the MAGMA code.

Figure 1 shows comparisons of total vapor pressures over molten alumina (m.p. = 2327 K) and molten silica (m.p. = 1996 K) with MAGMA code predictions. Figure 1a shows that our results are virtually identical to Krieger's (1966) calculations for alumina. Figure 1b shows that our results agree with the experimental measurements of Centolanzi and Chapman (1966) for molten tektite glass ($\sim$ 70% SiO_2 by weight) within their experimental uncertainties.

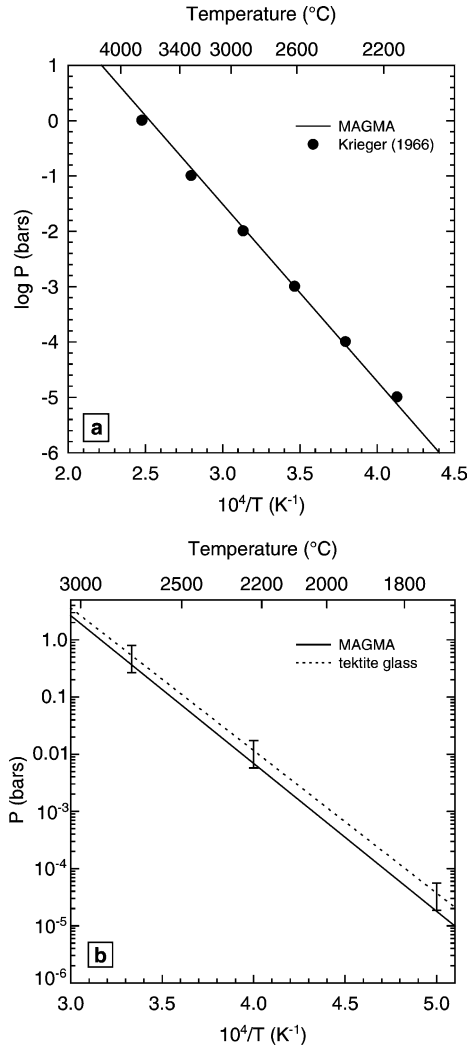

Fig. 1. Comparison of total vapor pressures calculated by the MAGMA code with (a) Krieger's (1966) calculations for molten alumina, and (b) the experimental measurements of Centolanzi and Chapman (1966) for molten tektite glass. The latter data have an uncertainty of a factor of 2, which is indicated by the error bars.

Figure 2 shows comparisons of the observed and calculated partial vapor pressures of oxide gases over pure molten oxides. Figure 2a shows Knudsen effusion mass spectrometry measurements of the AlO partial vapor pressure over molten alumina (Drowart et al., 1960; Farber et al., 1972;

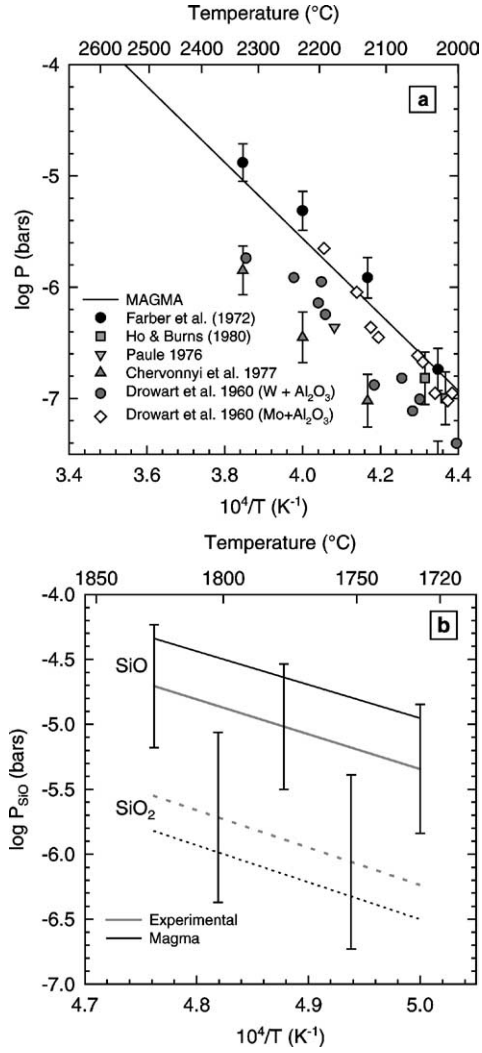

Fig. 2. (a) Comparison of the partial vapor pressure of AlO over liquid alumina calculated by the MAGMA code to experimental results from different groups (Drowart et al., 1960; Farber et al., 1972; Paule, 1976; Chervonnyi et al., 1977; Ho and Burns, 1980). The error bars are from the uncertainties of $\pm$8.4 kJ (Farber et al., 1972), $\pm$10.9 kJ (Chervonnyi et al., 1977), and $\pm$10.5 kJ (Ho and Burns, 1980) in the heats of formation of AlO gas. Drowart et al. (1960) give results for W and Mo Knudsen cells, but do not give uncertainties on them. Paule (1976) gives no uncertainties on his data. (b) Comparison of the partial vapor pressures of SiO and SiO_2 over molten silica calculated by the MAGMA code to experimental results from Shornikov et al. (1998, 2000). The error bars are from the uncertainties in the heats of formation of SiO ($\pm$19 kJ) and SiO_2 ($\pm$26 kJ) given by Shornikov et al. (2000).

Paule, 1976; Chervonnyi et al., 1977; Ho and Burns, 1980). Results from the MAGMA code plot well within the different experimental values. The observed and calculated partial vapor pressures of Al, Al_2O, and Al_2O_2 also agree well, but the predicted AlO_2 pressures are much lower than the observed values, which disagree among themselves. Figure 2b illustrates partial pressures of SiO and SiO_2 over molten silica. These were measured by Shornikov et al. (1998, 2000) using Knudsen effusion mass spectroscopy. The partial pressures of SiO and SiO_2 calculated with the MAGMA code agree with the data and are well within the experimental uncertainties.

Figures 3 and 4 demonstrate the excellent agreement between MAGMA results and experimental data for the Na_2O–SiO_2 and K_2O–SiO_2 binary systems. Zaitsev et al. (2000) measured sodium oxide and silica activities in Na_2O–SiO_2 melts by Knudsen effusion mass spectrometry over a range of compositions. Figure 3 is a plot of the Na_2O activity versus the Na_2O mole fraction in the melt. The sodium oxide activities computed by the MAGMA code agree with the data well within the experimental uncertainties. Figure 4 shows K (g) partial pressures over K_2O–SiO_2 melts from Plante (1979). We plot the K partial pressures measured over melts with 26.52–29.5 wt% K_2O ($X_{K_2O} = 0.187$ to 0.210). The agreement of MAGMA code results with these data and other (unplotted) data measured by Plante (1979) is excellent.

Figure 5 shows comparisons of calculated and observed partial vapor pressures for K, Na, and O_2 over multicomponent oxide melts. Figure 5a shows potassium partial pressures determined by Hastie et al. (1982b). They studied a variety of systems:

(1) K_2O–SiO_2,
(2) K_2O–Al_2O_3,
(3) K_2O–CaO–Al_2O_3–SiO_2,
(4) MHD channel slag, and
(5) illite.

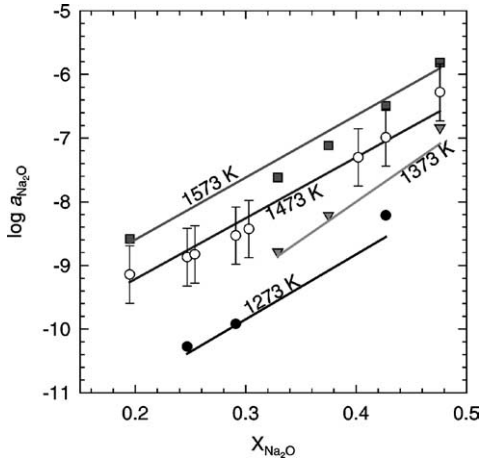

Fig. 3. Activity of Na_2O versus the mole fraction of Na_2O in the binary system Na_2O–SiO_2 calculated by the MAGMA code compared with experimental results from Zaitsev et al. (2000). The lines are isotherms from the MAGMA code, and points represent the experimental activities. The error bars on the 1473 K data are from the uncertainty in the partial molar Gibbs free energy of Na_2O. Errors at other temperatures should be of similar size but are not given by Zaitsev et al. (2000).

The compositions are given in Table 3. The MAGMA code predictions agree closely with the partial pressures over K_2O–SiO_2 and K_2O–Al_2O_3 and show good agreement with partial pressures over molten K_2O–CaO–Al_2O_3–SiO_2 and over molten MHD channel slag. Agreement with the potassium partial pressure over molten illite is poor, possibly due to the presence of volatiles such as S and H. Figure 5b shows the partial pressures of Na, K, and O_2 over Na_2O–K_2O–CaO–MgO–Al_2O_3–SiO_2 melts measured by Hastie and Bonnell (1985). The melt composition is shown in Table 3. The calculated MAGMA pressures are in good agreement with the Na and O_2 partial pressures, but the calculated K pressures are significantly lower than the experimental values.

We also compared MAGMA results to the data of Liu et al. (2001), who measured the FeO activity in smelting slags

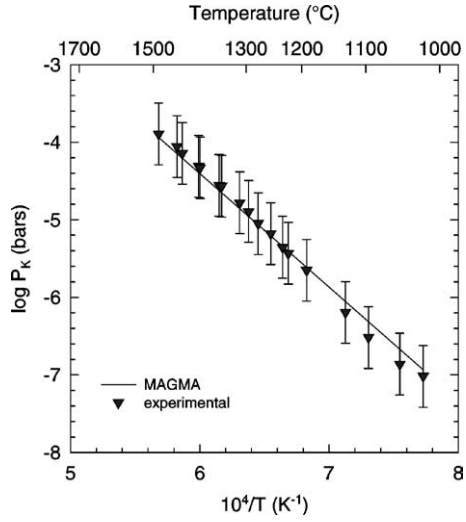

Fig. 4. Comparison of calculated vapor pressures of K (g) over the binary system K_2O–SiO_2 (26.52–29.5 wt% K_2O) with experimental results from Plante (1979). The points represents experimental data and the solid line is calculated by the MAGMA code. Plante (1979) estimates an uncertainty of ±40% in his K partial pressure data.

Table 3
Melt compositions for Fig. 5

Oxide (wt%)	1[a]	2[a]	3[a]	4[a]	5[a]	SRM glass[b]
Na_2O	–	–	–	0.5	0.2	12.75
K_2O	22.95	14.93	16.33	19.5	7.4	2.02
SiO_2	77.05	–	54.83	46.8	60.2	71.39
CaO	–	–	10.23	3.8	–	10.75
Al_2O_3	–	85.07	18.61	12.1	26.0	2.78
MgO	–	–	–	1.0	2.1	0.27
Fe_2O_3	–	–	–	14.3	4.4	0.04
Total	100.00	100.00	100.00	98.0	100.3	100.00

[a] Hastie et al. (1982b).
[b] Hastie and Bonnell (1985).

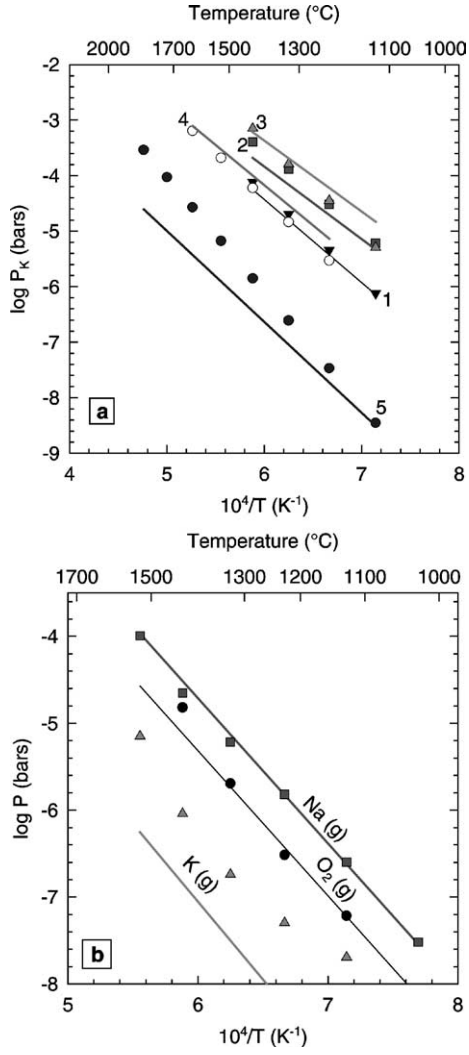

Fig. 5. (a) Vapor pressure of K over several systems as measured by Hastie et al. (1982b) (points) compared to calculated results from the MAGMA code (lines): (1) K_2O–SiO_2 (upside-down triangle); (2) K_2O–Al_2O_3 (square); (3) K_2O–Al_2O_3–CaO–SiO_2 (triangle); (4) MHD slag (open circle); (5) illite (filled circle) (see Table 3 for compositions). (b) Vapor pressure of Na, K, and O_2 over a synthetic glass (SRM glass, Table 3) measured by Hastie and Bonnell (1985) (points) compared with calculated results from the MAGMA code (lines). No uncertainties on the experimental data are given by Hastie et al. (1982b) or Hastie and Bonnell (1985).

of various compositions in the system MgO–CaO–SiO_2–Al_2O_3–FeO–Fe_2O_3. The slag systems were in equilibrium with iron metal, and the FeO activity was measured with an oxygen EMF cell. Our computed FeO activities are about one third of the experimental values because the FeO activity coefficients in the melts are 2.2 to 4.7, whereas the IMCC model can only match activity coefficients less than or equal to unity, as evident from Eq. (3).

Grossman et al. (2000) modeled the condensation and evaporation processes that formed the refractory inclusions in C3 chondrites. Figure 4 of Grossman et al.'s paper shows the calculated vapor pressure and composition of a CMAS (CaO–MgO–Al_2O_3–SiO_2) liquid as a function of P_{H_2}. Since the MAGMA code does not consider hydrogen in its calculations, we compare MAGMA results for this melt to the partial pressures at $P_{H_2} = 10^{-14}$ bars from Grossman et al., where the hydrogen should have little to no effect on the chemistry. We show the results in Table 4. Our computed total vapor pressure of 1.5×10^{-6} bars agrees well with the value of $\sim 1.7 \times 10^{-6}$ bars read from Fig. 4 of Grossman et al. (2000). Our calculated partial pressures are slightly smaller than the pressures from Grossman et al. (2000) but generally agree with them. The most deviant result is for P_{Al_2O} for which our calculated pressure is ~ 4 times smaller.

Table 4
Partial vapor pressures (bars)

Gas	Grossman et al. (2000)	MAGMA code
Mg	$\sim 2.0(-7)$[a]	1.4(−7)
MgO	$\sim 8.0(-10)$	3.6(−10)
Al	$\sim 9.0(-12)$	3.4(−12)
AlO	$\sim 9.0(-11)$	2.7(−11)
Al_2O	$\sim 10.0(-15)$	2.3(−15)
O	$\sim 3.0(-7)$	3.4(−7)
O_2	$\sim 3.0(-7)$	2.6(−7)
SiO	$\sim 9.0(-7)$	7.1(−7)
SiO_2	$\sim 7.0(-9)$	4.6(−9)
Ca	$\sim 1.5(-9)$	1.1(−9)
CaO	$\sim 2.5(-11)$	1.6(−11)
Total	$\sim 1.7(-6)$	1.5(−6)

[a] $2.0(-7) = 2.0 \times 10^{-7}$.

Richter et al. (2002) performed evaporation experiments to constrain the thermal evolution of type B calcium-, aluminum-rich inclusions in C3 chondrites and modeled their results using the thermodynamic model of Grossman et al. (2000), which is a modification of Berman's model (Berman, 1983; Berman and Brown, 1984). Figure 6a shows results from vacuum evaporation experiments performed by Richter et al. (2002), their modeled compositional trajectory at 2073 K, and the compositional trajectory calculated with the MAGMA code. The MAGMA code trajectory fits the data as well as the trajectory from Richter et al. (2002), and does a better job at low MgO contents. Figure 6b shows the activities of silica and MgO calculated by Richter et al. (2002) and by the MAGMA code. The calculated MgO activities match very well, but the SiO_2 activity calculated by the MAGMA code is about a factor of 3 lower than the value from Richter et al. (2002). They do not give experimental activity data for the compositions studied, nor have we been able to find any in the literature. Thus it is unclear whether the MAGMA results or the calculations of Richter et al. (2002) give a better match to the actual silica activities in the melts.

Wang et al. (2001) did isothermal evaporation experiments on synthetic oxide melts in a vacuum furnace at temperatures of 2073 and 2273 K. The synthetic oxide melt contained CI chondritic proportions of FeO, MgO, SiO_2, CaO, Al_2O_3, and TiO_2 doped with rare earth elements. They measured the mass lost from the samples and determined the composition of the residue. Hashimoto (1983) did similar isothermal vaporization experiments on a synthetic compo-

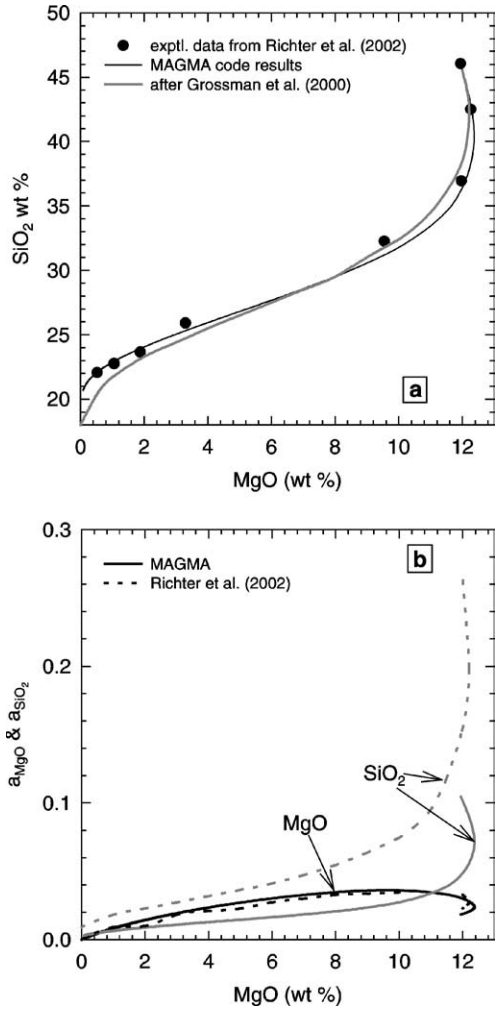

Fig. 6. Comparison of evaporation data and modeling by Richter et al. (2002) with MAGMA code calculations: (a) evaporation data (symbols) at 2073 K in a near vacuum of molten type B CAI-like compositions and compositional trajectory modeled after Grossman et al. (2000) compared to compositional trajectory calculated with the MAGMA code; (b) calculated activities of SiO_2 and MgO in their synthetic CAI from Richter et al. (2002) compared to activities calculated with the MAGMA code. No uncertainties on the experimental data are given by Richter et al. (2002).

sition with CI chondritic proportions of FeO, MgO, SiO_2, CaO, and Al_2O_3 for temperatures ranging from 1973 to 2273 K. We compare the fractional vaporization results of the MAGMA code to the residual compositions determined by Wang et al. (2001) and Hashimoto (1983) in Fig. 7. We do not distinguish between the 2073 and 2273 K data of Wang et al. (2001) because their data at different temperatures lie along the same curves as shown in Fig. 7 of Wang et al. (2001). We compare the data points to two curves computed by MAGMA for the temperatures 2073 and 2273 K. These lines are distinct in the plots of SiO_2, MgO, and FeO, but are identical for CaO, Al_2O_3, and TiO_2. The MAGMA calculations appear to slightly underestimate the abundance of SiO_2 and overestimate the abundance of MgO in the residues for less than 60% vaporization. If we take the experimental results at face value, our calculations will show slightly less Mg (mainly present as monatomic Mg) and slightly more Si (mainly present as SiO (g)) in the vapor than are actually present. At greater than $\sim 60\%$ vaporization, the results from MAGMA are nearly identical to the data points. Our calculations show good agreement with the data for FeO from both Hashimoto (1983) and Wang et al. (2001). The MAGMA calculations are nearly identical to the experimental results for CaO, Al_2O_3, and TiO_2 below $\sim 60\%$ vaporization. For higher degrees of vaporization, the MAGMA results slightly overestimate the abundances of the refractory elements in the melt. If the experimental results represent complete chemical equilibrium, then the MAGMA code will predict less Ca, Al, and Ti (mainly present as Ca, Al, AlO, and TiO_2 gases) in the vapor than are present.

We also compared the results of the MAGMA code to vaporization experiments on a lunar basalt performed by Markova et al. (1986). These researchers evaporated a lunar aluminiferous basalt (Apollo 16 sample #68415,40) in a Knudsen cell. We calculate a liquidus temperature for this basalt of ~ 1240 K. They heated the basalt continuously from 1273 to 2500 K and measured the vapor composition and pressure above the liquid basalt. The major vapor species that the researchers observed (Na, K, Fe, FeO, SiO, Mg, Ca, CaO, TiO, TiO_2, Al, AlO) are qualitatively similar to the major species predicted by the MAGMA code. Our results are also in agreement with their volatility sequence: Na, K > Fe > Si > Mg > Ca, Ti > Al. Markova et al. (1986) used the Hertz–Knudsen equation:

$$\alpha_s P_{vap} = m\sqrt{\frac{2\pi RT}{M}}, \tag{11}$$

where α_s is the vaporization coefficient ($= 1$ for equilibrium, < 1 for kinetic inhibition), P_{vap} is the equilibrium vapor pressure, m is the vaporization rate ($g\,cm^{-2}\,s^{-1}$), R is the ideal gas constant, T is temperature in Kelvins, and M is the molecular weight of the vapor, to determine the vaporization rate. They also calculated the mass percent vaporized and the residual melt composition over the temperature range they studied. Figure 8 shows the residual compositions as points plotted versus the extent of vaporization. The lines in the figure are isothermal results from the MAGMA code for temperatures of 2000 and 2400 K. However, Markova et al. (1986) heated the basalt continuously from 1273 to 2473 K so the earlier stages of fractional vaporization occurred at lower temperatures. The MAGMA code computations at lower temperatures therefore better match the residual compositions at low degrees of vaporization, which can be seen in Fig. 8b for FeO.

The MAGMA code has also been used effectively to model the differential ablation of metals (particularly Na, K, Ca, Mg, and Fe) from meteors and cosmic dust entering the Earth's upper atmosphere (McNeil et al., 1998a, 1998b, 2002; Eska et al., 1999; Von Zahn et al., 1999, 2002). These workers find that the fractional vaporization predicted by the MAGMA code matches the observed enrichments of

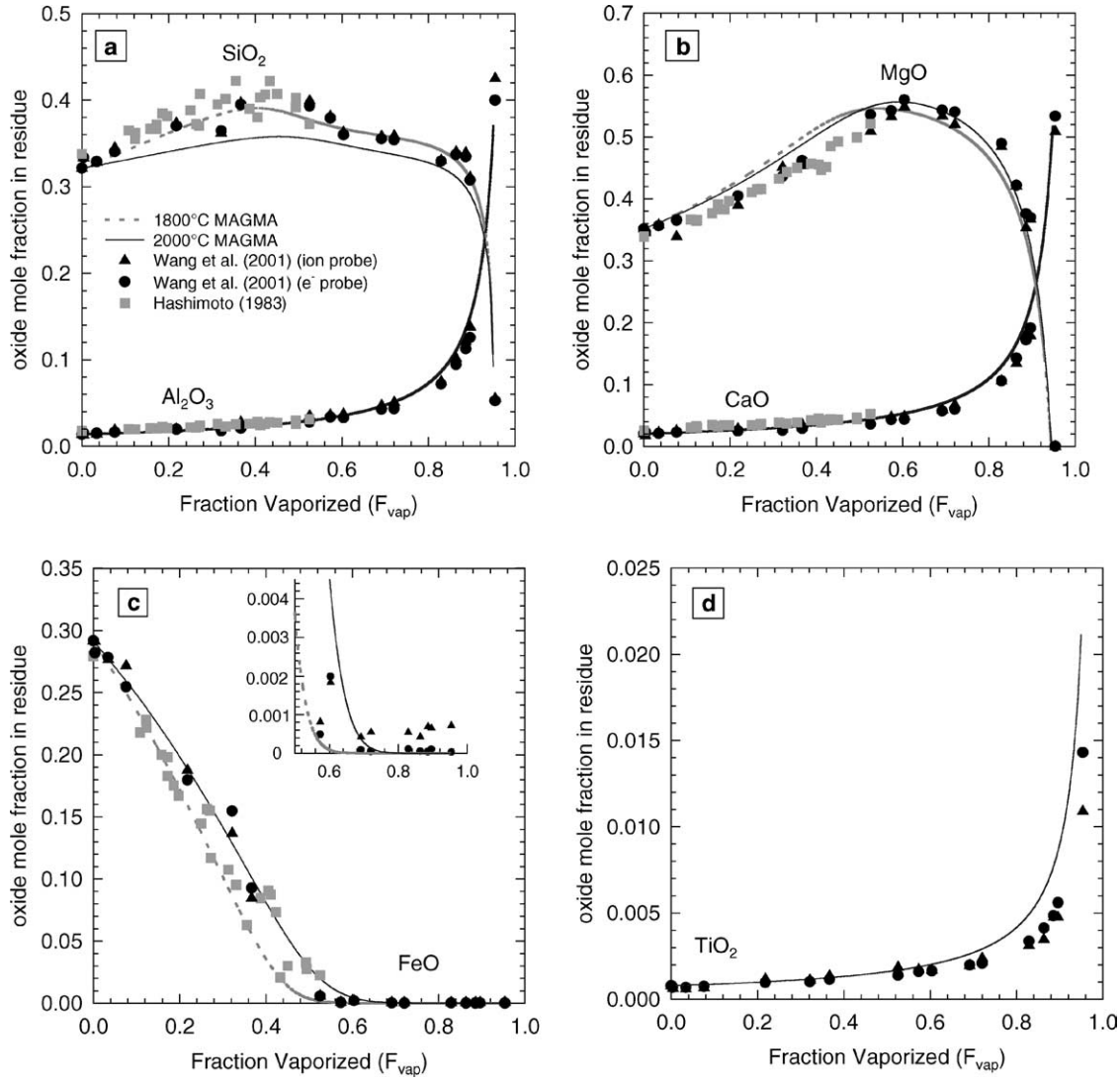

Fig. 7. Comparison of residual melt compositions for synthetic systems calculated by the MAGMA code to the results of evaporation experiments from Hashimoto (1983) and Wang et al. (2001). (a) SiO_2 and Al_2O_3, (b) MgO and CaO, (c) FeO, (d) TiO_2, mole fractions in the residue versus fractional extent of vaporization. No uncertainties on the experimental data are given by Hashimoto (1983). Uncertainties given by Wang et al. (2001) are smaller than the point size.

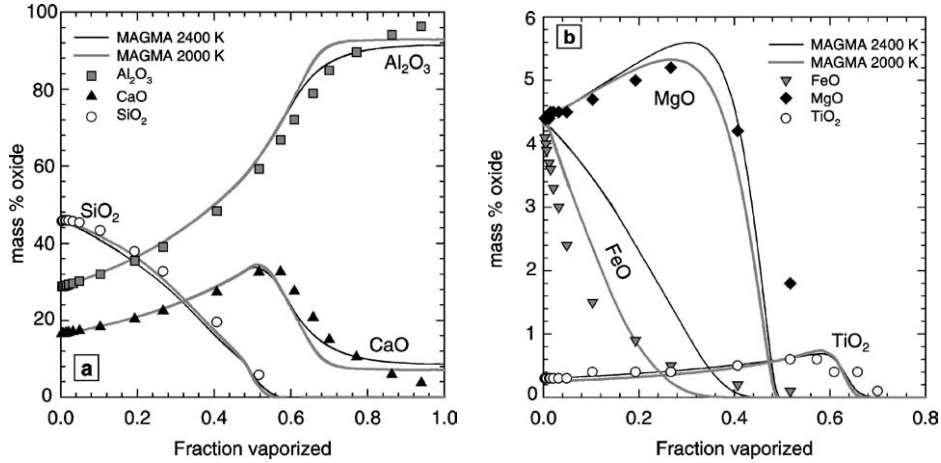

Fig. 8. Comparison of residual melt compositions of fractional vaporization of Apollo 16 lunar basalt 65415,40 by Markova et al. (1986) to calculations by the MAGMA code. (a) SiO_2, CaO, and Al_2O_3, (b) FeO, MgO, and TiO_2 weight percent in the residue versus fractional extent of vaporization. No uncertainties on the experimental data are given by Markova et al. (1986).

Na and K relative to Ca, Mg, and Fe in the Earth's upper atmosphere.

2.4. Temperature

We computed fractional vaporization with the MAGMA code over a wide range of temperatures (1700–3000 K). In general, our figures present results for the temperature range 1700–2400 K. Lower temperatures were not considered because the MAGMA code assumes a completely molten system. Calculations must therefore be made at temperatures greater than the liquidus temperatures (T_{liq}) of the lavas. Calculations presented here that are below the respective liquidus temperatures of the komatiite, dunite, and Type B1 CAI in Table 5 are extrapolations made to show trends. The liquidus temperatures of the alkali basalt, komatiite, and dunite given in Table 5 were calculated using the MAGfox code developed by John Longhi of Lamont Doherty Geophysical Observatory. This code is based on parameterization of liquidus boundaries and crystal–liquid partition coefficients in the model basaltic system olivine–plagioclase–pyroxene–SiO_2 (Longhi, 1987, 1991; Longhi and Pan, 1989). The liquidus temperature of the tholeiite is taken from Williams et al. (2001) and the liquidus temperature of the B1 CAI is an average value for type B CAIs from Stolper (1982). The liquidus temperature calculated by the MAGfox code for the tholeiitic basalt is lower than the Williams et al. (2001) value by ~ 70 K. This code cannot be used for CAIs since olivine is not the liquidus phase.

Table 5
Model compositions

Wt. oxide	Tholeiite	Alkali basalt	Komatiite	Dunite	Type B1 CAI
SiO_2	50.71	44.80	47.10	40.20	29.10
MgO	4.68	11.07	29.60	43.20	10.20
Al_2O_3	14.48	13.86	4.04	0.80	29.60
TiO_2	1.70	1.96	0.24	0.20	1.30
Fe_2O_3	4.89	2.91	12.80	1.90	0
FeO	9.07	9.63	0	11.90	0.60
CaO	8.83	10.16	5.44	0.80	28.80
Na_2O	3.16	3.19	0.46	0.30	0.18
K_2O	0.77	1.09	0.09	0.10	0.10
Other	1.62[a]	1.45[b]	0.27[c]	0.70[d]	0.10[e]
Total	99.91	100.12	100.04	100.10	100.01
T_{liq} (K)[f]	1433[g]	1504	1838	1954	1823[h]
Ref.	[1]	[2]	[3]	[4]	[5]

[a] MnO (0.22%), H_2O (1.04%), P_2O_5 (0.36%).
[b] MnO (0.17%), H_2O (0.73%), P_2O_5 (0.55%).
[c] MnO (0.22%), P_2O_5 (0.05%).
[d] MnO (0.20%), H_2O (0.40%), P_2O_5 (0.10%).
[e] Cr_2O_3 (0.04%), NiO (0.06%).
[f] See text for details.
[g] From Williams et al. (2001).
[h] From Stolper (1982).
[1] Murase and McBirney (1973).
[2] Carmichael et al. (1974, p. 501 #1).
[3] Arndt (2002, personal communication to B. Fegley).
[4] MacDonald (1972).
[5] MacPherson et al. (1988).

Table 6
Hot spot temperatures from Galileo observations

Hot spot	Orbit	Best T (K)[a]	Area (km^2)	Ref.
Pillan	C9	1870	0.11	Davies et al. (2001)
Pele	I27	1760 ± 210	< 0.00005	Lopes et al. (2001)
Kanehekili-N	G7	1660	> 0.006	McEwen et al. (1998)
Unnamed 22 °N, 238°	E11	1620	0.0002	McEwen et al. (1998)
Surt	–[b]	> 1470	30	Marchis et al. (2002)
Amirani	G8	1675	0.00006	McEwen et al. (1998)

[a] Uncertainties are given where available.
[b] Ground-based observation from the Keck Observatory.

The temperature range studied here includes the temperatures derived for some hot spots on Io (e.g., Pele and Pillan) and for large volcanic outbursts (e.g., Surt, Marchis et al., 2002). We list some of these high temperature observations in Table 6.

2.5. Lava compositions

We did calculations for 109 rock compositions. The majority of these compositions are basalts of various types, including ocean island basalts (OIBs), mid-ocean ridge basalts (MORBs), alkali basalts, and continental tholeiitic basalts. Other rock types studied included rhyolite, komatiite, dunite, peridotite, meimechite, picrite, alkaline, and ultrapotassic mafic rocks, and calcium–aluminum rich inclusions (CAIs). A list of all compositions studied is given in Appendix A. In this paper, we present graphical results for the compositions listed in Table 5: a terrestrial tholeiitic basalt used in modeling by Williams et al. (2001), an alkali basalt, a Barberton-type komatiite, a dunite, and an Allende type B1 inclusion. The results for these compositions are representative of all of the compositions studied. All compositions that contained volatiles and minor or trace elements were renormalized on a volatile-free and minor and trace element free basis for our computations.

The compositions studied were chosen on the basis of the suggestions found in the literature for lava compositions on Io. While there is little spectroscopic data about the lava compositions, observed temperatures $\geqslant 1400$ K suggest silicate compositions (e.g., Carr, 1986; Veeder et al., 1994; Davies, 1996; Stansberry et al., 1997; Lopes-Gautier et al., 1997). The lithosphere of Io must also be strong enough to support mountains ~ 10 km high, which suggests a silicate composition (Nash et al., 1986; Spencer and Schneider, 1996). Basaltic volcanism is frequently referred to in the literature (e.g., Keszthelyi and McEwen, 1997b; Davies, 1996; Veeder et al., 1994; Hapke, 1989; Stansberry et al., 1997). Most terrestrial volcanism is basaltic in nature, with eruption temperatures of 1400–1600 K (Carmichael et al., 1974). On Io, approximately 20 hot spots have been observed with temperatures that fall into this range (McEwen et al., 1998). By analogy with Earth, these temperatures are suggestive of basaltic volcanism. Additional higher temperature observations, ranging from 1600–1850 K (see Table 6), could also

be caused by basaltic volcanism. A superheated basaltic lava ascending rapidly from deep within the mantle (McEwen et al., 1998) could produce such temperatures. However, in order to produce a basaltic lava with a temperature of 1870 K, the lava must ascend from ∼ 1000 km depth with little heat loss (Kargel et al., 2003b).

While it is possible for lavas to ascend from such depths, a more likely explanation for the high (> 1600 K) temperatures is that the lavas have a higher liquidus temperature than basalts. One broad type of lavas that could produce such temperatures are ultramafic lavas, which have high magnesium contents and therefore high melting temperatures. The most commonly mentioned ultramafic lavas are komatiites, which were erupted during the Archaean on Earth some 3.8 to 2.5 billion years ago when the thermal output of the Earth was more similar to the thermal output of Io today (McEwen et al., 1998; Williams et al., 2001).

Komatiites are highly magnesian (typically 20–30%) rocks with low TiO_2 (< 1%) and low alkali contents ($Na_2O + K_2O$ < 1%) (Arndt et al., 1995). The komatiite shown in our figures is a Barberton-type komatiite. Williams et al. (2001) suggest the Commondale komatiite as the best analog for ionian lavas because it is the only known komatiite that contains orthopyroxene, which has been tentatively identified on Io (Geissler et al., 1999b). Compared with our other komatiite compositions, the Commondale komatiite has a much larger Na/K ratio and is significantly more iron-deficient and aluminium-rich. We therefore prefer to show the results for the Barberton komatiite, which is more representative of other komatiites.

Other ultramafic compositions that have been suggested include dunite (Keszthelyi and McEwen, 1997a), meimechites (Zolotov and Fegley, 1999) and picrites (Matson et al., 1998). Dunites are ultramafic rocks that are essentially pure olivine and contain roughly equal amounts of SiO_2 and MgO. From their model of magmatic differentiation on Io, Keszthelyi and McEwen (1997a) predict that the mantle of Io should be primarily dunite. Meimechites are very similar to dunites in SiO_2 and MgO content and have $Na_2O + K_2O$ < 1%, and TiO_2 > 1%. They typically have Na/K ratios less than one (Arndt et al., 1995). Except for alkali abundances, results for meimechites are very similar to the results for dunite. Meimechites and alkali picrites are part of the same suite of rocks found together in the Meimecha-Kotui Province of Siberia with an age of ∼ 248 million years (Arndt et al., 1995). Picrites are slightly more alkali-rich ($Na_2O + K_2O$ > 1%) and less magnesium-rich (∼ 18–30%) than meimechites. Picrites also generally have Na/K ratios less than one (Arndt et al., 1995). Our computed results for picrites are very similar to komatiites, which have similar MgO contents.

Alternatively, as suggested by J.S. Kargel (Kargel and Fegley, 2002; Kargel et al., 2003a, 2003b), the high temperatures may indicate lavas of some ultrarefractory ceramic composition, similar to the coarse-grained CAIs found in carbonaceous chondrites. Calcium, aluminum-rich inclusions are enriched in refractory elements such as Ca, Al, and Ti. We considered 5 different types of CAIs: fluffy type A, type B1, type B2, type C, and the MUM3 inclusion from the Murchison CM2 chondrite (see Appendix A). While there is no single CAI that is representative of all CAIs, we show in this paper figures for the type B1 inclusion, which has the median vapor pressure of all of the CAIs studied.

3. Computational results

3.1. Total vapor pressure over the lavas

Figure 9 shows the total vapor pressure of the five compositions in Table 5 as a function of temperature. Figure 9a illustrates the initial vapor pressures of the model compositions. The initial vapor pressure is the vapor pressure over

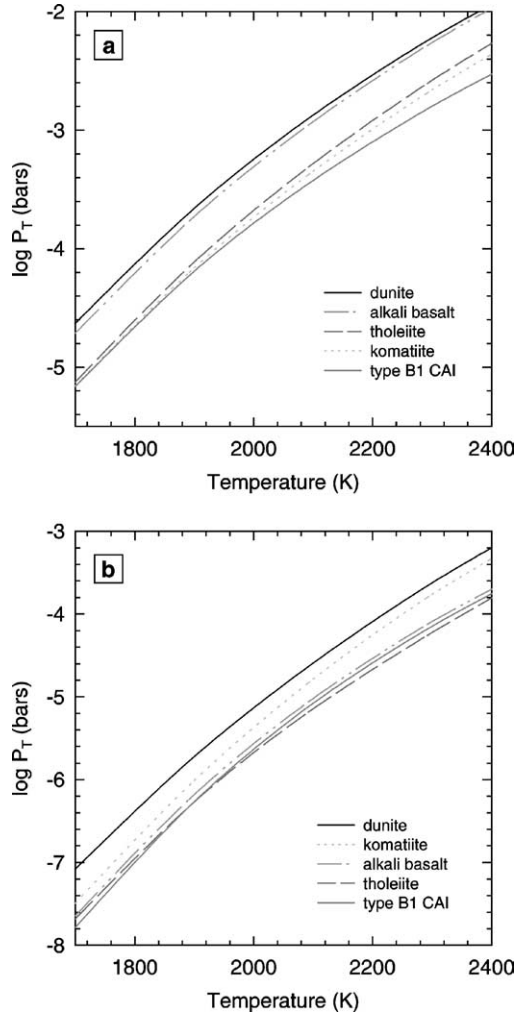

Fig. 9. (a) Initial vapor pressures for the lava model compositions over the temperature range from 1700–2400 K. The initial vapor pressure is the sum of the vapor pressures of all of the gases in equilibrium with the lava, and is dominated by the alkalis. (b) Vapor pressures of the lava model compositions after the loss of all of the alkalis. The total vapor pressures and the range of total vapor pressures decrease after the loss of the alkalis.

the lava prior to any fractional vaporization, i.e., at 0% vaporization. Figure 9b shows the vapor pressures of the model compositions after the loss of all of the alkalis (Na and K) by fractional vaporization. For the tholeiitic basalt, all of the alkalis are lost after 64% of the original basalt vaporizes. Alkali loss from the other lavas occurs after 54% (alkali basalt), 22% (komatiite), 2% (dunite), and 10% vaporization (type B1 CAI). Sodium is typically lost much more rapidly than potassium: for the tholeiite basalt, Na is lost by 17% vaporization; alkali basalt by 10%; komatiite by 1.5%; dunite by 0.6%; and the B1 CAI by 0.5%.

The initial vapor pressures of dunite and the alkali basalt shown in Fig. 9a are nearly identical. The tholeiite and the komatiite vapor pressures are very similar to one another but are less than those of dunite and the alkali basalt. The Allende type B1 CAI has an initial vapor pressure similar to the tholeiite and the komatiite at low temperatures. As temperature increases, the vapor pressure over the CAI does not increase as much as the vapor pressures of the tholeiite and the komatiite.

Table 7 lists vapor pressures and vapor pressure equations at 1900 K for the 5 model compositions given in Table 5 and lists the ranges of initial vapor pressures for each composition (tholeiite, alkali basalt, etc.) from our calculations for the 109 rocks listed in Appendix A. The vapor pressures for all of the compositions are significantly higher than the atmospheric pressure of Io ($\sim$ 1–10 nanobars, Spencer and Schneider, 1996). As can be seen in the figures and in the table, the total vapor pressures for different rock types are not unique for each type. The petrologic type with the smallest range of pressures is tholeiitic basalt. There are two separate but overlapping ranges for continental tholeiites and oceanic tholeiites (MORBs). The oceanic tholeiites are slightly more alkaline than the continental tholeiites and therefore have higher vapor pressures. The range of vapor pressures for ocean island basalts completely encompasses the combined range of all tholeiites. The range of vapor pressures for komatiites encompasses continental tholeiites. The range for CAIs is even larger, encompassing the komatiites and all tholeiites. We find therefore that the total vapor pressure is not diagnostic of bulk composition of the different rock types.

Table 7
Vapor pressure over model compositions (in bars)

Composition	$A^{a,b}$	$B^{a,b}$	Pressure[b] (bars)	Range at 1900 K[c]	
			at 1900 K	minimum	maximum
Basalt					
Tholeiites	4.719	−16761	7.72(−5)[d]	5.52(−5)	7.72(−5)
MORBs	–	–	8.23(−5)[e]	7.79(−5)	1.01(−4)
Alkalis	4.716	−16037	1.87(−4)	–	–
OIBs	–	–	1.26(−4)[e]	3.59(−5)	4.43(−4)
Komatiites	4.480	−16404	6.89(−5)	2.08(−5)	9.73(−5)
Dunite	4.618	−15724	2.19(−4)	–	–
CAIs	3.890	−15373	6.46(−5)	1.98(−5)	1.62(−4)

[a] $\log_{10} P_{\text{vap}}$ (bars) $= A + B/T$.
[b] For model compositions listed in Table 5.
[c] For compositions listed in Appendix A.
[d] $7.72(-5) = 7.72 \times 10^{-5}$.
[e] Median value.

3.2. Initial vapor compositions over the magmas

3.2.1. Temperature-dependent trends

Figure 10 presents the initial vapor compositions for the model lavas over the temperature range 1700–2400 K. As can be seen, the vapor composition varies with temperature. Some general trends are apparent for all of the compositions. The three most abundant gases are nearly always Na, O_2, and O. At 1700 K, monatomic Na gas is approximately 3 orders of magnitude more abundant than other metals in the vapor, O_2 is ~ 2 orders of magnitude more abundant, and O is ~ 1 order of magnitude more abundant. The abundances of Na and O_2 are relatively temperature-independent, whereas the abundance of O increases sharply with temperature.

Monatomic sodium gas accounts for more than 99% of the total sodium in the vapor. The rest of sodium is distributed between NaO, Na^+, Na_2, and Na_2O in order of decreasing abundance. The gas phase chemistry of potassium is similar to that of sodium, with K gas making up more than 99% of total potassium. The second most abundant potassium gas is K^+, making up $< 0.2\%$ of total potassium, followed by KO, K_2O and K_2. Several of these Na- and K-bearing gases have mole fractions smaller than 10^{-5} and are not shown in Fig. 10. There is substantial thermal ionization of the alkali gases, particularly Na gas. The only ionization products included in our calculations are Na^+ and K^+ because sodium and potassium have the lowest first ionization potentials of all of the elements considered. In nearly all cases, the Na^+ ion is more abundant than K^+.

The distribution of the other metals in the gas is as follows. Monatomic Fe gas and FeO have similar abundances at low temperatures. As temperature increases, Fe becomes more abundant than FeO. Silicon is distributed between Si, SiO, and SiO_2, with SiO always more abundant than SiO_2 for the temperature range considered here. Monatomic Si gas is negligible. Magnesium is distributed between Mg gas and MgO, with Mg more abundant than MgO. Essentially all titanium is in TiO_2 gas. Monatomic Ti gas and TiO have much lower abundances. Monatomic Ca gas constitutes 85–90% of all calcium, and the remainder is CaO. Aluminum occurs primarily as AlO, with very minor amounts of Al, AlO_2, Al_2O_2, and Al_2O, in decreasing order of abundance.

3.2.2. Potential compositional diagnostics

We found two important trends in vapor chemistry that are potentially diagnostic of lava composition. The first trend is that monatomic Mg gas is much more abundant in the vapor over ultramafic lavas and Ca, Al-rich lavas than over basaltic lavas. This point can be seen by comparing Figs. 10a and b with Figs. 10c–e. Magnesium gas is less abundant than SiO_2 in the vapor over tholeiitic and alkaline basalts

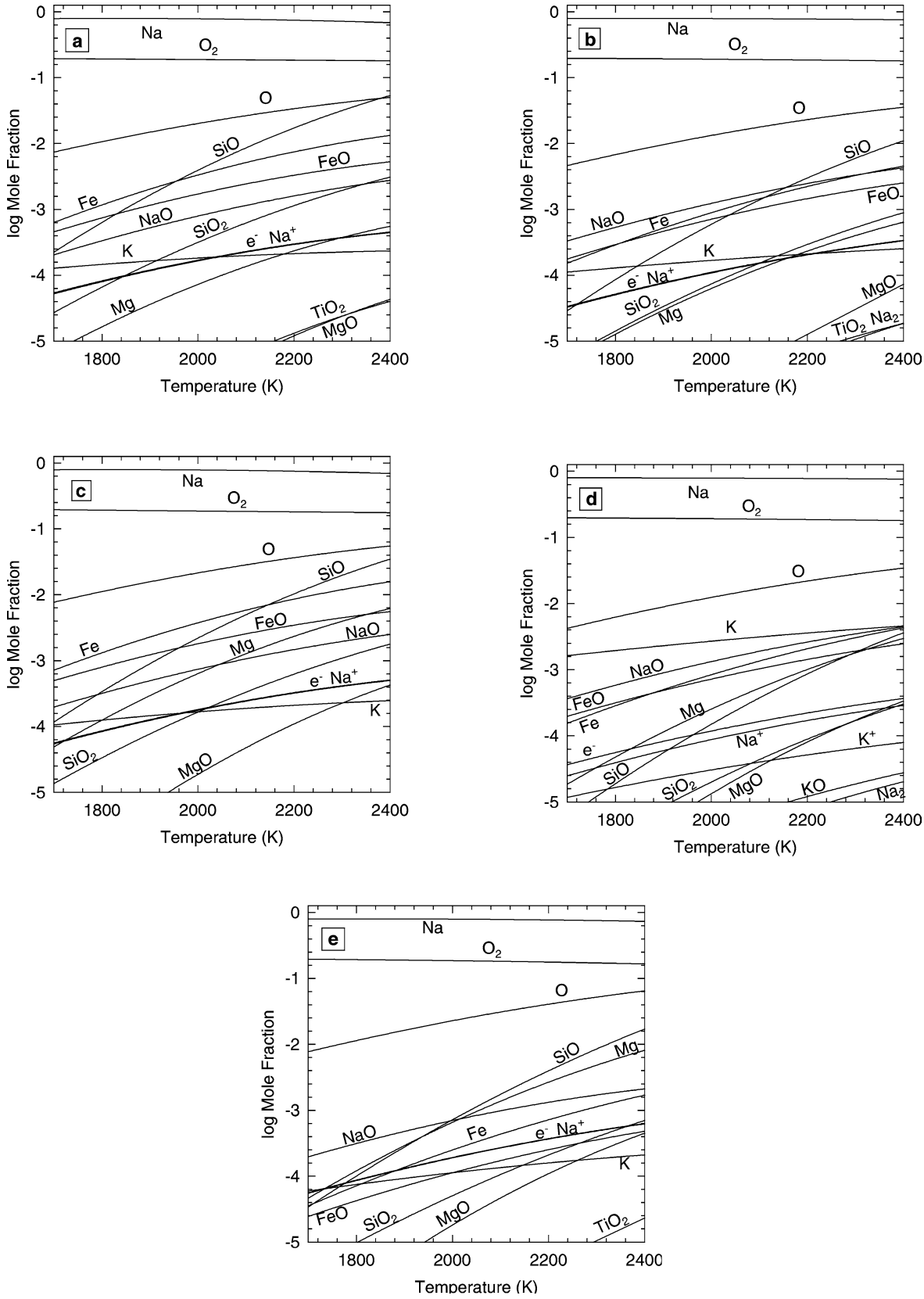

Fig. 10. Temperature-dependent vapor compositions (mole fractions) for the lava model compositions: (a) tholeiite, (b) alkali basalt, (c) komatiite, (d) dunite, (e) Allende type B1 CAI.

but more abundant than SiO_2 in the vapor over the Barberton komatiite lava, molten dunite and the molten Type B1 CAI. The dunite and Allende CAI are so silica-poor that Mg is even more abundant than SiO in the vapor over these lavas. The second trend is that K_2O is more abundant than K^+ in the vapor over lavas enriched in potassium, such as orendite from the Leucite Hills in Wyoming (see Appendix A). At 1900 K, K_2O is actually the second most abundant gas in the vapor over orendite, following only monatomic K gas.

3.3. Fractional vaporization

The vapor over hot lavas on Io may be partially or completely lost, e.g., by being blown away, and may not recondense back into the cooling lava. Consequently, the bulk composition and mineralogy of an erupted lava may change due to loss of vaporized elements. We modeled this possibility by computing the changes in the equilibrium composition of vapor and lava during continuous loss of vapor, a process known as fractional vaporization.

Our results showing the effect of fractional vaporization on composition of the vapor and lava are displayed in Figs. 11 and 12. These calculations were done at 1900 K which was chosen because it is close to the highest temperature so far derived from observations of a hot spot on Io (1870 K, Davies et al., 2001).

Figure 11 illustrates the partial vapor pressures of the most abundant gases over the five model lava compositions given in Table 5. Sodium is the most volatile element in most lavas and is lost first. For example, all sodium, which is dominantly present in the vapor as Na gas, is lost from the tholeiitic basalt lava by 17% vaporization (see Fig. 11a). Sodium does not appear in Figs. 11b–e because it is lost after small amounts of the lavas have vaporized, as previously stated.

Potassium is generally the second most volatile element after sodium, although occasionally, such as in Figs. 11a and b, iron is lost before potassium. The large volatility difference between Na and K is manifested by a preferential partitioning of Na into the vapor, i.e., the $(Na/K)_{vapor}/(Na/K)_{lava}$ ratio is much greater than unity except for a few unusual lavas (see Appendix A). Consequently, fractional vaporization depletes lavas in Na relative to K, and decreases the Na/K ratios in the residual lavas and the vapor in equilibrium with them.

As total gaseous Fe rapidly decreases in abundance, either SiO or Mg becomes the most abundant gas, depending upon how ultramafic the system is. In systems that have Mg/Si ratios > 1, such as dunite, Mg gas will be more abundant than SiO. For instance, compare Fig. 11c-komatiite and d-dunite. Dunite has a Mg/Si atomic ratio of ~ 1.6 and the komatiite has a ratio of ~ 0.94. Accordingly, Mg gas is more abundant than SiO in the vapor over dunite, whereas SiO is initially more abundant than Mg gas above the komatiite. As the amount of vaporization increases, the Mg/Si ratio of the komatiite increases, so that SiO, O_2, and O decrease in abundance (SiO is always more abundant than O_2 and O), whereas Mg increases in abundance until it reaches a peak, and then decreases. At its peak abundance, Mg is more abundant than SiO for those alkali basalts and ultramafic compositions that have Mg/Si ratios > 0.3, e.g., Figs. 11b–e. This is not true for tholeiitic basalts and the more felsic compositions such as rhyolite and andesite, which have much smaller Mg/Si ratios in the lava.

In Figs. 11 and 12, the total percentage of lava vaporized does not correspond to the same molar percentage of SiO_2 lost in each case. Since each lava has a different bulk composition and silica content, removing all of the silica from each lava will leave different fractions of the original lavas behind. Comparing the different plots in Fig. 12, one sees that as the lavas become increasingly mafic (e.g., basalt to dunite), SiO_2 is lost more slowly. That is, a given percentage of SiO_2 vaporized from an ultramafic lava corresponds to a higher total percentage of the lava vaporized than for a mafic composition. For example, a loss of 80% of all SiO_2 from a tholeiitic basalt corresponds to $\sim 60\%$ total vaporization. A similar loss of SiO_2 from a komatiite corresponds to $\sim 75\%$ total vaporization even though the tholeiite and komatiite shown in Figs. 11 and 12 have similar SiO_2 contents. Therefore, while silicon is initially more abundant in the vapor, when more magnesium is present in the melt, it is vaporized preferentially over silicon.

The graphs presented in Figs. 11 and 12 only show the results for fractional vaporization at one temperature. What are the differences in fractional vaporization with changes of temperature? One difference is that silica is lost more rapidly at higher temperatures. For example, 20% total vaporization of a tholeiite at 2100 K is equivalent to losing about 50% of its original silica content, whereas at 1900 K, 20% total vaporization equals less than 20% SiO_2 vaporization. Conversely, iron is lost more slowly at higher temperatures.

Figure 12 shows the evolution of melt bulk composition versus the degree of vaporization. The mole fraction of FeO (liq) peaks after complete loss of sodium, and the mole fraction of silica peaks before FeO (liq) is completely lost. These peaks generally occur up against the y-axis of the plots in Fig. 12 for very small degrees of vaporization. Both oxides then steadily decrease with continued vaporization in all cases. Due to the high magnesium content, the silica content of dunite is fairly constant throughout most of the fractional vaporization, though it does decrease slightly from 10 to 80% vaporized. At $\sim 90\%$ vaporized, which is off the graph, the SiO_2 (liq) content of dunite drops dramatically. Conversely, the mole fractions of MgO, CaO, Al_2O_3, and TiO_2 in the lavas increase with increasing vaporization, except in the case of the CAI. There is so little volatile material (e.g., Na, K, Fe) present in the CAI that Si and Mg are quickly vaporized, with MgO being lost first from the lava.

However, in the other lavas, MgO (liq) displays behavior similar to Mg gas with both increasing to a maximum and then decreasing as fractional vaporization proceeds. A comparison of the plots in Figs. 11 and 12 for each lava shows

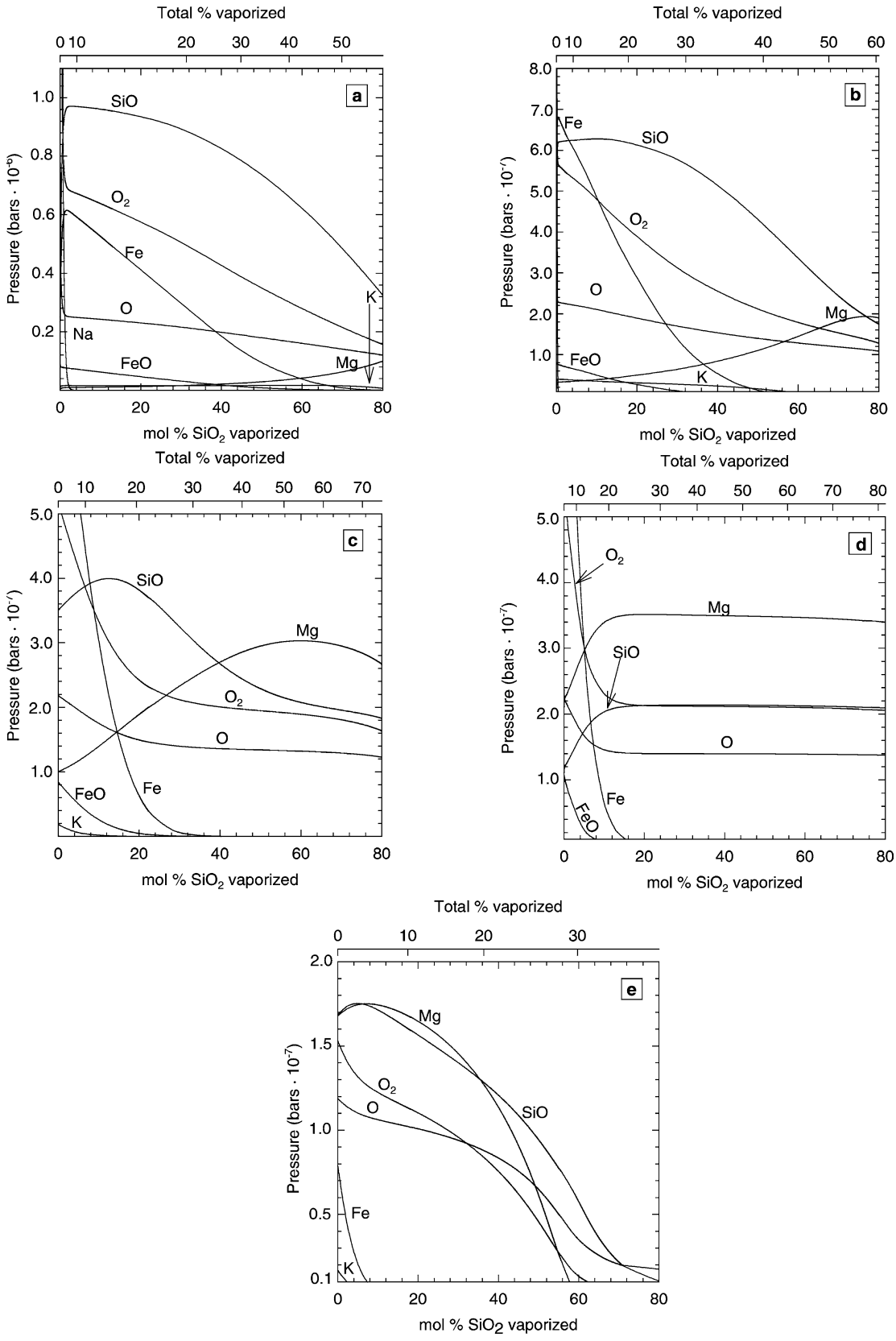

Fig. 11. Effect of fractional vaporization at 1900 K on composition of the vapor for: (a) tholeiite, (b) alkali basalt, (c) komatiite, (d) dunite, and (e) Allende type B1 CAI. The total molar % vaporized is shown separately for each composition.

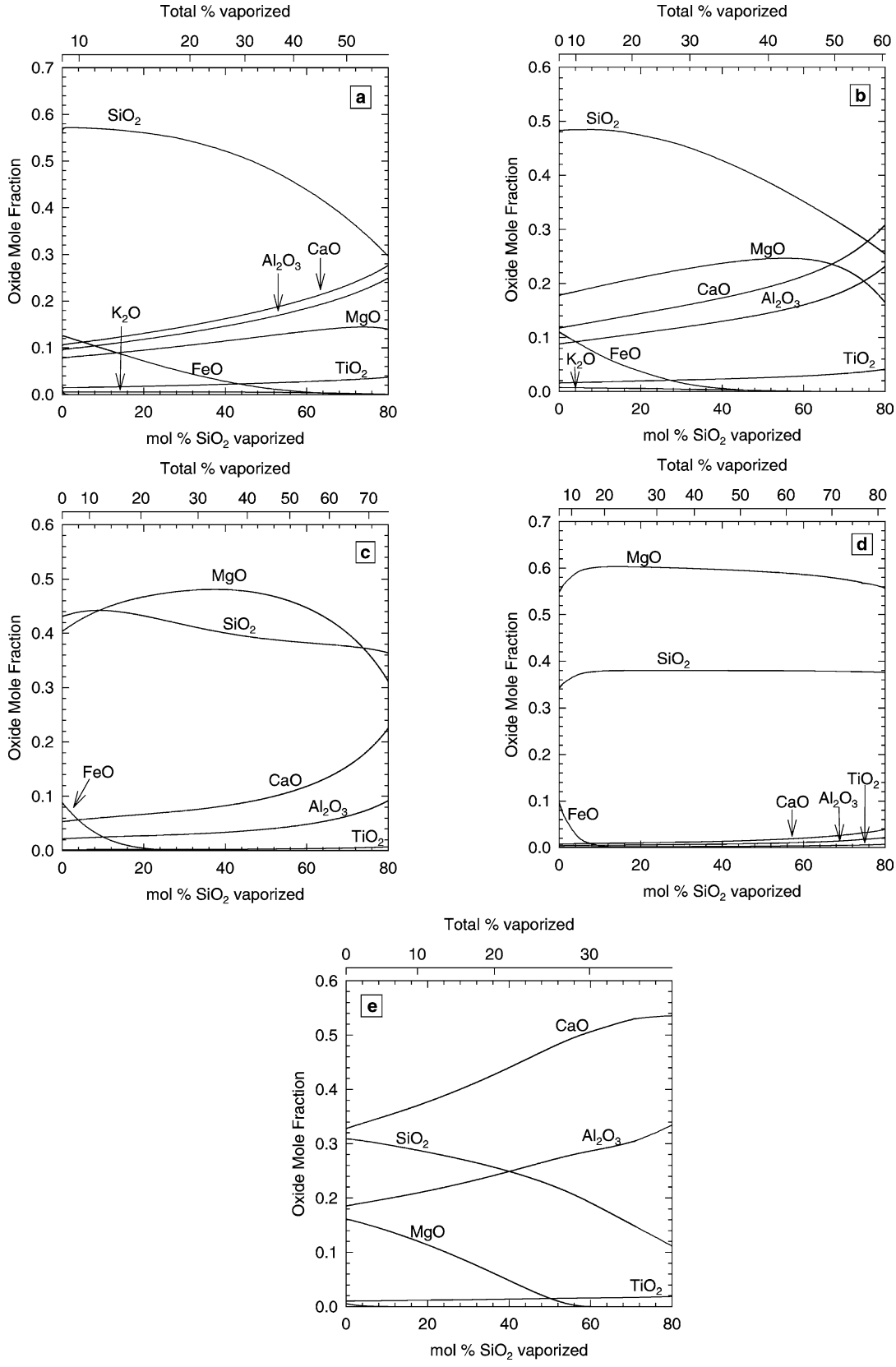

Fig. 12. Effect of fractional vaporization at 1900 K on composition of the residual lava for: (a) tholeiite, (b) alkali basalt, (c) komatiite, (d) dunite, and (e) Allende type B1 CAI. The total molar % vaporized is shown separately for each composition.

that the peak abundance of Mg gas occurs at a later stage than the peak abundance of MgO (liq). This is most easily seen in the plots for the komatiite: Figs. 11c and 12c. In general, the effect of modest degrees of fractional vaporization is to decrease the concentrations of Na_2O, K_2O, FeO, and SiO_2 in the residual lava and to increase the concentrations of MgO, CaO, Al_2O_3, and TiO_2 in the lava. The effects of fractional vaporization on liquidus temperatures and crystallization of the partially vaporized lavas are described by Kargel et al. (2003a, 2003b).

4. Discussion and applications to Io

4.1. Evaporative loss of alkalis and other volatiles during volcanic eruptions

As discussed above, our calculations predict evaporative loss of the alkalis and other elements from erupting lavas. For example, the tholeiitic basalt lava in Figs. 11a and 12a is completely depleted in Na after 17% of the lava is vaporized. The depletion sequence and percentage of lava vaporized for complete loss of other elements is K (64%), Fe (72%), Mg (73%), Si (77%), Ti (87%), Ca $\sim$ Al ($>$ 99.9%). Our calculated vaporization sequence for tholeiite basalt agrees with that determined experimentally by DeMaria et al. (1971) for vaporization of lunar basalt 12022 with the exception that their sequence for the most refractory elements is Ca, Al, and Ti. As shown in Figs. 7 and 8, our calculated vaporization sequences also agree with those measured by Hashimoto (1983), Wang et al. (2001), and Markova et al. (1986) for synthetic oxide mixtures and lunar basalt 68415,40. The agreement between our calculations and experimental results of other groups is encouraging. However, will lavas erupted onto Io's surface actually lose alkalis and other elements because of vaporization?

At present this question cannot be answered with certainty because we do not have geochemical analyses of ionian rocks or remote sensing observations of Na and K vaporization from volcanic vents and lava flows on Io. We can, however, draw analogies to volatile-depleted basalts from other extraterrestrial bodies. Lunar basalts and basaltic achondrite meteorites (eucrites) are depleted in alkalis, and evaporative loss has been suggested to explain their volatile element depletions (e.g., O'Hara et al., 1970; Mittlefehldt, 1987; Lodders, 1994). The basaltic achondrites are believed by many to come from Asteroid 4 Vesta, but this identification is not firm. Thus we prefer to consider only lunar basalts to address the question posed above. Another reason for considering lunar basalts is that the Moon has several similarities to Io.

The Moon and Io have about the same size (1737 vs. 1821 km radius), mass (7.35×10^{22} vs. 8.93×10^{22} kg), and density (3344 vs. 3529 kg m^{-3}). Io's heat flow is significantly higher than the Moon's and hence Io remains volcanically active today while lunar volcanism ceased several billion years ago. Volcanism on both satellites occurred (or occurs) in low pressure tenuous atmospheres, that have (or plausibly had) total pressures much lower than the vapor pressures of the lavas being erupted.

When the Apollo lunar samples were examined it was noticed almost immediately that lunar basalts are depleted in alkalis and other volatiles relative to their typical concentrations in terrestrial basalts (e.g., Gast and Hubbard, 1970). Evaporative loss of alkalis and other volatiles was one of the possibilities suggested to explain the data (O'Hara et al., 1970). Vaporization experiments on lunar and terrestrial basalts showed that Na, K, and Rb were lost within hours at temperatures of 1323–1673 K in vacuum (DeMaria et al., 1971; Naughton et al., 1971; Gibson and Hubbard, 1972; Storey, 1973). Ringwood and Essene (1970) advanced an alternative explanation based on their geochemical and petrological studies of Apollo 11 samples that the Moon is depleted in volatiles relative to Earth. The model of a volatile-poor Moon became the consensus viewpoint and remains so today.

Nevertheless the vaporization experiments on lunar and terrestrial basalts showed that alkalis are rapidly lost from basaltic lavas. Liquidus temperatures of lunar basalts (1423–1673 K) are typically lower than the highest temperatures observed for lavas on Io (1620–1870 K, see Table 6). Consequently, the partial vapor pressures of Na and K over ionian lavas should be significantly higher than those over lunar lavas because vapor pressures increase exponentially with temperature (see Fig. 9 and Table 7). Assuming a volcanism rate equal to (or greater than) the present rate, Io has recycled its entire crust and mantle at least 80 times (Kargel et al., 2003a, 2003b). Even if fractional vaporization is less than 100% efficient, some of the alkalis could be evaporated each time a lava erupts, and the cumulative effect may be large.

Gibson and Hubbard (1972) raised several objections to evaporative loss of volatiles from lunar lavas, which we now consider for ionian lavas. They suggested that vaporization "would cause only a skin-effect depletion" of volatiles without affecting the rest of the lava flow. Gibson and Hubbard's argument may be valid for relatively quiescent lava flows, but they acknowledge that it is probably irrelevant for lavas that are vigorously mixed by processes such as convection, splattering, or fountaining or that have gas bubbling within the lava. Volatile loss may actually be fairly efficient during vigorous, high-temperature eruptions such as those observed at Pillan Patera in summer 1997 (Williams et al., 2001) or at Surt in February 2001 (Marchis et al., 2002).

A second objection raised by Gibson and Hubbard (1972) is that no Na-rich volcanic condensates are found on the Moon. In contrast to the Moon, Io does have surficial deposits, which could be condensates from volcanic gases. These deposits include SO_2 frost and various allotropes of elemental sulfur (Spencer and Schneider, 1996). Volcanic deposits of halite (NaCl), sodium sulfate (Na_2SO_4) and sodium sulfide (Na_2S) have been suggested by sev-

eral groups over the past thirty years (Fegley and Zolotov, 2000, and references therein). Finally, Gibson and Hubbard (1972) argued that lunar lava flows might have cooled before sodium was lost. As opposed to the Moon, some lava flows on Io are both large (30 km^2) and hot (> 1470 K) such as that at Surt (see Table 6). Additionally, lava lakes such as Pele, which has had a high surface temperature (> 1400 K) for many years (Radebaugh et al., this issue), may be vaporizing continuously. Thus, while the objections raised by Gibson and Hubbard (1972) may be relevant to volatile loss on the Moon, these arguments do not seem to be relevant to Io.

Furthermore, there is some observational evidence that alkalis are emitted from volcanoes on Io. The green emissions observed by Galileo over volcanic centers plausibly arise from the D line of sodium vapor (Bouchez et al., 2000; Geissler et al., 1999a), and Lellouch et al. (2003) reported the observation of volcanic NaCl gas. Observations of Na- and K-bearing gases from actively erupting volcanoes have not been reported, but would be worth doing, especially over Pele.

4.2. Upper limits for abundances of metals in Io's atmosphere and plasma torus

With the exception of Na and K, none of the predicted metal vaporization products have yet been found in Io's extended atmosphere or in the Io plasma torus (IPT). Based upon non-detection of the neutral atoms, Na et al. (1998) gave upper limits relative to sodium for several metals in Io's atmosphere and IPT (see Table 8). Sodium is less abundant in the lavas than Si, Fe, Ca, or Al but is enriched in Io's extended atmosphere and the IPT relative to these more abundant, but less volatile metals. For example, the Si/Na atomic ratios in the five model lava compositions are 7.2 (alkali basalt), 8.3 (tholeiite), 52.8 (komatiite), 69.1 (dunite), and 83.4 (Type B1 CAI). The CI chondritic Si/Na atomic ratio is comparable to these values and is 17.4 (Lodders 2003). In contrast, the Si/Na upper limit of < 0.014 in Io's atmosphere is ~ 510 times smaller than the tholeiite Si/Na ratio and ~ 3800 times smaller than the komatiite Si/Na ratio. Likewise, the Fe/Na, Ca/Na, and Al/Na ratios in the tholeiitic basalt are 1.8, 1.5, and 2.8, while the upper limits in Io's extended atmosphere are < 0.038, < 0.001, and < 0.008, respectively.

Table 8
Relative abundances of the metals in the gas with respect to sodium[a]

Element	Na et al. (1998)	Tholeiite	Alkali basalt	Komatiite	Dunite	Type B1 CAI
Na	1.000	1.000	1.000	1.000	1.000	1.000
K	0.10[b]	2.11(−4)[c]	1.88(−4)	1.87(−4)	2.92(−3)	1.19(−4)
Al	< 0.008	8.77(−9)	2.68(−9)	5.79(−9)	3.98(−10)	1.31(−8)
Si	< 0.014	2.35(−3)	3.49(−4)	1.27(−3)	8.31(−5)	3.79(−4)
Ca	< 0.001	8.25(−9)	4.15(−9)	1.03(−8)	7.91(−10)	1.60(−7)
Ti	< 0.014	1.68(−6)	6.67(−7)	2.08(−7)	3.31(−8)	6.79(−7)
Fe	< 0.038	4.10(−3)	1.26(−3)	4.53(−3)	1.26(−3)	2.64(−4)

[a] $T = 1900$ K.
[b] Brown (2001).
[c] $2.11(-4) = 2.11 \times 10^{-4}$.

Our results are consistent with these upper limits, which do not rule out fractional vaporization of metal-bearing gases from hot lavas on Io. This point is demonstrated in Table 8 where metal/Na ratios in the vapor over the five model lava compositions at 1900 K are compared to the upper limits from Na et al. (1998). They do not give an upper limit for Mg, so this metal is not included in the comparison in Table 8. The metal/Na ratios in the vapor over any of the lavas are less than the upper limits for the same metal/Na ratio for Io's atmosphere. For example, the vapor initially evolved from the tholeiitic basalt lava has a Si/Na ratio $= 2.35 \times 10^{-3}$, which is six times lower than the Si/Na upper limit of < 0.014. The Si/Na ratios in the vapor over the other lavas range from 1.27×10^{-3} (komatiite) to 8.31×10^{-5} (dunite). The metal/Na ratios in the vapor over lavas decrease as the lava temperatures decrease and increase as the lava temperatures increase. The metal/Na ratio over a lava also increases during fractional vaporization as Na is continuously vaporized and lost. Thus, at 1900 K the Si/Na ratio in the vapor over the tholeiitic basalt lava increases until it exceeds the upper limit for Io's atmosphere at $\sim 7\%$ vaporization.

Na et al. (1998) based their upper limits on observations of the neutral atoms. However, neutral atoms may constitute only a small fraction of the total metal abundance in the gas. We calculated the equilibrium distribution of Si between neutral monatomic Si and Si^+, Si^{+2}, Si^{+3}, and Si^{+4} as a function of temperature at different total pressures. At 10^{-9} bars total pressure, the equilibrium distribution shifts from 100% neutral monatomic Si gas at 1000 K, to 12.3% Si and 87.7% Si^+ at 3000 K, to 99.6% Si^{+2} and 0.4% Si^+ at 8500 K. We use thermal ionization as a proxy for the actual physical processes that take place to illustrate our point, namely that the ionization processes in Io's extended atmosphere and the IPT may cause a large fraction of the total Si, Fe, and Mg in the gas phase to be present as ionized species instead of the neutral atoms that were the focus of Na et al. (1998). In other words, their upper limits to metal/Na ratios may be much less restrictive than they appear.

4.3. Fractional vaporization of alkali elements and the abundance of alkalis in Io's extended atmosphere

Sodium and potassium were discovered around Io about 30 years ago (Brown, 1974; Trafton, 1975). A large amount of work has been done on their sources and sinks, which are still incompletely understood (Spencer and Schneider, 1996). One important prediction of our work is that fractional vaporization may produce the observed Na/K ratio in Io's extended atmosphere (Brown, 2001). This ratio is 10 ± 3 (Brown, 2001) and is close to the CI chondritic Na/K atomic ratio of 16.0 (Lodders, 2003). The Na/K ratios in many of the rock types we studied are also close to the at-

mospheric Na/K ratio (within a factor of 2–3). In contrast, the Na/K ratios in the vapor over basaltic, komatiitic, and other lavas suggested for Io are 10–1000 times larger than the atmospheric value (see Appendix A). This indicates that the Na/K ratio found over hot spots could be decidedly different than the bulk atmospheric value.

Potassium has a lower ionization potential than Na, so ionization reduces the abundance of neutral monatomic K more than that of neutral monatomic Na, and increases the Na/K atmospheric ratio. However, our calculations predict that Na is more volatile than K and is lost before K for almost all of the lavas we modeled. This predicted trend agrees with experimental studies by DeMaria et al. (1971), Storey (1973), Shimaoka et al. (1994), and Yu et al. (2003) in which the same trend was observed. Fractional vaporization of our tholeiite lava yields the Na/K atmospheric ratio after $\sim 7\%$ vaporization. Only 0.1% fractional vaporization is needed for the vapor over the Barberton komatiite lava to match the atmospheric Na/K ratio. Unlike the other metals, the Na/K ratio in the vapor is insensitive to temperature, so the amount of fractional vaporization required to match the atmospheric value of Brown (2001) does not change much with temperature.

It is also possible that some lavas on Io are K-rich. The vapor over these lavas is closer to the atmospheric Na/K value. We modeled molten orendite, which is an ultrapotassic mafic rock found in the Leucite Hills, WY. The vapor over this lava has an initial Na/K ratio of ~ 2.8, which would be shifted toward the atmospheric value by ionization. In any case, spectroscopic measurements of the Na/K ratio in the gas over active hot spots are needed to test whether or not fractional vaporization of lavas (basalts or komatiites) or eruption of K-rich lavas may be responsible for the atmospheric Na/K ratio on Io.

4.4. Chemistry of silicon monoxide gas

Our results predict that SiO is the major Si-bearing gas over the lavas. This prediction agrees with mass spectrometric studies of the vapor composition over molten lunar basalts (DeMaria et al., 1971; Markova et al., 1986), which show that SiO is the major Si-bearing gas. Other mass spectrometric studies show that SiO is the major Si-bearing gas over molten silica (Shornikov et al., 1998), molten forsterite (Mg_2SiO_4, Nichols et al., 1998), and binary melts of silica with other metal oxides including Al_2O_3, BaO, CaO, FeO, GeO_2, or MnO (Stolyarova, 2001).

Silicon monoxide is also the most widespread Si-bearing molecule in space. It has strong IR bands at 4 μm (first overtone) and 8 μm (fundamental) and lines throughout the millimeter region. Silicon monoxide gas is observed in the atmospheres of cool stars and their circumstellar outflows, molecular clouds, star-forming regions, and supernovae. The SiO mole fractions that are observed range from about 10^{-5} in cool M giant stars (Tsuji et al., 1994) to about 10^{-10} in molecular clouds (Le Picard et al., 2001). The SiO column densities are about 10^{11}–10^{12} cm^{-2} in diffuse and spiral-arm clouds (Lucas and Liszt, 2000), and about 10^{14}–10^{15} cm^{-2} in molecular clouds, star-forming regions and cool stars (Groesbeck et al., 1994; Hatchell et al., 2001; Minh et al., 1992). For comparison, the SiO column densities (mole fractions) in the vapor over the tholeiite lava in Fig. 10a range from $\sim 10^{17}$ cm^{-2} ($x_{SiO} \sim 10^{-3.6}$) at 1700 K to 10^{19} cm^{-2} ($x_{SiO} \sim 10^{-2.7}$) at 1900 K, and those over the komatiite lava in Fig. 10 range from $10^{16.8}$ cm^{-2} ($x_{SiO} \sim 10^{-3.9}$) at 1700 K to $10^{18.7}$ cm^{-2} ($x_{SiO} \sim 10^{-3.2}$) at 1900 K. These SiO column densities and mole fractions are larger than those observed in space. We thus single out SiO and strongly recommend searching for it over active volcanic regions on Io.

As long as lava is being erupted, the SiO abundance around active volcanic vents should be close to the equilibrium partial pressure of SiO above the lava. Once the vent stops erupting and lava solidifies, the SiO abundance is no longer regulated by the presence of the coexisting lava. The destruction of SiO in a volcanic gas plume or vapor cloud is plausibly initiated by absorption of UV light shortward of 300 nm (Podmoshenskii et al., 1968; Vorypaev, 1981; Matveev, 1986)

$$\mathrm{SiO} + h\nu \rightarrow \mathrm{Si} + \mathrm{O}, \quad \lambda < 300\ \mathrm{nm}. \tag{12}$$

Photoionization of SiO requires photons with much higher energies of 11.584 ± 0.011 eV (Baig and Connerade, 1979), and is probably a less important sink. The Si atoms formed by reaction (12) can react with O_2 (g) to regenerate SiO via

$$\mathrm{Si}\left(^3\mathrm{P}\right) + \mathrm{O}_2 \rightarrow \mathrm{SiO} + \mathrm{O}, \tag{13}$$

which has the rate constant (Le Picard et al., 2001)

$$k = 1.72 \times 10^{-10} (T/300\ \mathrm{K})^{-0.53} \exp(-17/T)\ \mathrm{cm}^3\,\mathrm{s}^{-1} \tag{14}$$

and is plausibly the most important loss process for Si (g). The O_2 in reaction (13) should be abundant in Pele-like volcanic plumes (e.g., Moses et al., 2002a) and in the vapor evolved from hot lavas (see Figs. 10a–e). Alternatively Si atoms could be lost via the three body reactions:

$$\mathrm{Si} + \mathrm{Si} + \mathrm{M} \rightarrow \mathrm{Si}_2 + \mathrm{M}, \tag{15}$$

$$\mathrm{Si} + \mathrm{O} + \mathrm{M} \rightarrow \mathrm{SiO} + \mathrm{M}, \tag{16}$$

which are highly exothermic, but probably very slow in Io's low density atmosphere. Reactions such as

$$\mathrm{Si} + \mathrm{SiO} \rightarrow \mathrm{Si}_2\mathrm{O}, \tag{17}$$

$$\mathrm{Si} + \mathrm{SiO}_2 \rightarrow \mathrm{SiO} + \mathrm{SiO}, \tag{18}$$

$$\mathrm{Si} + \mathrm{Si}_2 \rightarrow \mathrm{Si}_3 \tag{19}$$

are possibly important sinks for monatomic Si gas, but are probably less efficient than reaction (13). If S_2 is present the formation of SiS (g),

$$\mathrm{Si} + \mathrm{S}_2 \rightarrow \mathrm{SiS} + \mathrm{S} \tag{20}$$

may compete with reaction (13). Although the exothermic reaction

$$SiO + O + M \rightarrow SiO_2 + M \quad (21)$$

is also a possible sink for SiO, it is probably very slow on Io. Other possible sinks such as

$$SiO + SiO \rightarrow Si + SiO_2 \quad (22)$$

are endothermic by several hundred kJ, and probably are unimportant by comparison with reactions (13) and (20). Condensation of SiO via the reaction

$$SiO + \text{dust} \rightarrow SiO\ (\text{condensed}) \quad (23)$$

or the condensation of silica

$$SiO_2 + \text{dust} \rightarrow SiO_2\ (\text{silica}) \quad (24)$$

are probably the ultimate loss processes for SiO (g). It is hard to evaluate the efficiency of these condensation reactions. Arguing by analogy with the behavior of NaCl (Moses et al., 2002b), we suggest that an observable amount of SiO (g) should be present above active volcanic regions, but that condensation will deplete SiO on a time scale of minutes to hours after volcanic activity has ceased. Solid SiO and silica are more refractory than NaCl and SiO should be depleted by condensation more rapidly than predicted for NaCl (see Fig. 9 of Moses et al., 2002b).

4.5. Vaporization fluxes and column densities of metallic vapors

We can relate the calculated partial vapor pressures of Na, K, SiO, Fe, and other metallic vapors to their vaporization fluxes using Eq. (11). The temperature dependent fluxes ($cm^{-2}\,s^{-1}$) for O, O_2, e^-, and the most abundant metallic vapors over our tholeiitic lava are listed in Table 9. These calculations assume that the vaporization coefficient $\alpha_s = 1$, and the actual fluxes may be smaller if $\alpha_s < 1$. We discuss this possibility below in the section about kinetic constraints.

Table 9
Calculated molecular flux ($cm^{-2}\,s^{-1}$) of the most abundant vapor species over a tholeiitic lava

Species	1550 K	1700 K	1900 K
Na	1.00(17)[a]	7.94(17)	7.67(18)
O_2	2.10(18)	1.66(17)	1.58(18)
e^-	6.51(14)	1.10(16)	2.42(17)
O	5.65(14)	8.84(15)	1.76(17)
Fe	1.64(13)	4.03(14)	1.29(16)
FeO	1.30(13)	2.56(14)	6.45(15)
SiO	3.01(12)	1.60(14)	1.19(16)
NaO	1.26(13)	2.43(14)	6.20(15)
K	1.01(13)	9.84(13)	1.22(15)
Na^+	3.02(12)	5.20(13)	1.15(15)
SiO_2	4.08(11)	1.65(13)	9.26(14)
Mg	1.70(11)	6.69(12)	3.49(14)
K^+	1.21(11)	1.50(12)	2.37(13)

[a] $1.00(17) = 1.00 \times 10^{17}$.

As an example, using Table 9, we estimate that $\sim 9 \times 10^{28}$ SiO molecules may have been vaporized during the large volcanic outburst observed in August 1986 ($T = 1550$ K, duration = 4.5 hours, diameter = 15 km, Spencer and Schneider, 1996). The SiO column density during the outburst, assuming local hydrostatic equilibrium, may have been about $\sim 2 \times 10^{15}$ SiO per cm^2. This is 0.04–10% of the SO_2 column densities of $\sim 2 \times 10^{16}$ to $\sim 5 \times 10^{18}$ cm^{-2} for large volcanic plumes on Io (Moses et al., 2002a).

4.6. Reactions of metallic vapors with other species in Io's atmosphere and in volcanic gases

Our calculations model vaporization of high temperature lavas into a vacuum. However, Io's atmosphere is not a vacuum but a mixture of SO_2 and other gases, such as SO and O_2 which are photolysis products of SO_2 (e.g., see Moses et al., 2002a, and references therein) with a total pressure of $\sim$ 1–10 nanobars. The chemical and dynamical interactions of the background atmosphere with metallic vapors from hot lavas are likely complex and are not modeled here.

It is also possible that at least some of the vapors from high temperature lavas could mix and react with hot volcanic gases. What would happen in this case? As long as lava is being erupted and has not solidified, the partial pressures of Na, K, SiO, FeO, Fe, Mg, and other metal-bearing gases will be regulated by the presence of the lava. Once the volcanic vent stops erupting and lava solidifies, the metal-bearing vapors may be depleted by thermochemical and/or photochemical reactions with S-, O-, and Cl-bearing species in the volcanic gas. Complete consideration of this chemistry is beyond the scope of this paper.

However, our prior modeling of alkali and chlorine chemistry (Fegley and Zolotov, 2000) indicates that thermochemical reactions would produce significant amounts of NaCl and KCl gases and smaller amounts of $(NaCl)_2$ and $(KCl)_2$ gases. Monatomic Na and K gases also persist unless the Cl/(Na + K) atomic ratio is greater than unity. Depending on the bulk O/S atomic ratio in the gas, the alkalis could condense as Na_2S, Na_2SO_4, NaCl, and KCl droplets or crystals. The dependence of this chemistry on temperature, pressure, and elemental abundances in the O, S, Cl, Na, K system is discussed in detail by Fegley and Zolotov (2000).

We have also made two sets of preliminary chemical equilibrium calculations for a Pele-like vent ($T = 1760 \pm 210$ K, Lopes-Gautier et al., 1997) to model the chemistry of Si, Fe, and Mg. We previously showed that the nominal total pressure for Pele is ~ 0.01 bars (Zolotov and Fegley, 2001) and we used this total pressure in both computations. The elemental abundances used for O, S, Cl, Na, and K in both calculations are 1.521/1.0/0.05/0.05/0.005, respectively. These values are the same as those in Moses et al. (2002b). Different Si/Na, Mg/Na, and Fe/Na ratios appropriate for the vapor over tholeiitic lava at 1760 K (see Fig. 10a) or for the vapor over komatiite lava at 1860 K (see Fig. 10c) were taken. The total Si/Na, Mg/Na, and Fe/Na ratios in the vapor over

tholeiitic lava at 1760 K are 6.0×10^{-4}, 1.5×10^{-5}, and 2.0×10^{-3}, respectively. In this model we find that gaseous silicon is dominantly SiO (95.3%) with smaller amounts of SiO_2 (3.5%) and SiS (1.2%). Monatomic Mg (53.1%) makes up about half of gaseous magnesium with the balance divided between $MgCl_2$ (33.8%), MgS (9.3%), MgCl (3.4%), and MgO (0.4%). The major Fe-bearing gases are Fe (57.3%), $FeCl_2$ (27.5%), FeS (10.8%), FeO (2.5%), and FeCl (1.9%).

The total Si/Na, Mg/Na, and Fe/Na ratios in the vapor over the komatiite lava at 1860 K are 4.4×10^{-5}, 1.4×10^{-5}, and 1.8×10^{-4}, respectively. The gas phase speciation of Si, Mg, and Fe is similar to that found for the tholeiitic lava. Silicon monoxide (95.9%) is the major Si-bearing gas with SiO_2 (3.1%), and SiS (1.0%) comprising the rest. Magnesium is mainly monatomic Mg (53.0%) and $MgCl_2$ (35.5%) with the remainder in MgS (6.5%), MgCl (4.4%), and MgO (0.6%). Monatomic Fe (59.1%) and $FeCl_2$ (28.7%) are again the major Fe-bearing gases with FeS (7.0%), FeO (2.7%), and FeCl (2.5%) making up the rest.

These two computations reinforce our suggestion to search for SiO (g), which remains the major Si-bearing gas even if vapor from the hot lava reacts with sulfur and chlorine species in volcanic gases. Our results also suggest that efforts should be made to detect $MgCl_2$ and $FeCl_2$ vapors above active and very hot volcanic vents such as those at Pele and Pillan.

4.7. Kinetic constraints on lava vaporization

The equilibrium vapor pressures calculated by MAGMA code may be higher than the actual vapor pressures above lavas on Io if vaporization of the lavas is kinetically inhibited. In this case, the vaporization coefficient α_s in Eq. (11) is less than unity. This situation often arises during vaporization of solids into vacuum, i.e., during Langmuir vaporization (Paule and Margrave, 1967). The vaporization coefficient α_s (or α_V in some literature) is given by the ratio of the equilibrium (P_{vap}) and observed (P_{obs}) vapor pressures:

$$\alpha_s = P_{obs}/P_{vap}. \quad (25)$$

The vaporization coefficient is temperature dependent because the equilibrium and observed vapor pressures are also temperature dependent. Equilibrium vapor pressures are often measured using Knudsen effusion cells, while the vapor pressures from the Langmuir method are generally less than the equilibrium values. Thus P_K and P_L, which stand for Knudsen and Langmuir pressures, respectively, sometimes replace P_{vap} and P_{obs} in Eq. (25). As far as we can tell, there are no experimental data available for any of the lavas considered here. Thus we cannot simply give α_s values based on experimental data.

Instead we surveyed the literature for α_s values for oxides and silicates. Table 10 presents our results, which are mainly for solids. The data show two key points, first, that α_s values increase at higher temperatures and second, that α_s values are less than unity for solids in most cases. Some of the data are contradictory. For example, Peleg and Alcock (1974) reported $\alpha_s = 0.24$–0.49 for corundum (α-Al_2O_3 solid) at 1800–1900 K, Krönert and Boehm (1972) reported $\alpha_s = 0.14$ at 2000 K, and Wolff and Alcock (1962) give $\alpha_s = 0.067$ at 2000 K. Nevertheless the two trends noted above appear valid.

Table 10
Vaporization coefficients for oxides and silicates

Oxide	T (K)	α_s	Reference
Al_2O_3 (s)	1800–1900	0.24–0.49	Peleg and Alcock (1974)
	2000	0.14	Krönert and Boehm (1972)
	2000	0.067	Wolff and Alcock (1962)
	2195	0.08	Farber et al. (1972)
	2290	~ 0.80	Alcock and Peleg (1967)
	2310[a]	0.3 ± 0.05	Burns (1966)
Al_2O_3 (l)	2310[a]	1.0	Burns (1966)
MgO (s)	1800	0.25	Peleg and Alcock (1974)
	1900	0.4	Peleg and Alcock (1974)
	1820–1960	~ 0.25	Alcock and Peleg (1967)
	2273	0.09	Krönert and Boehm (1972)
	1873–2173	0.12–0.22	Hashimoto (1990)
SiO_2 (s)	1823–1983	0.022 ± 0.008	Nagai et al. (1973)
	1700–1950	0.022 ± 0.003	Shornikov et al. (1999)
	1833–1958	0.11–0.015	Hashimoto (1990)
SiO_2 (liq)	2173–2373	0.038–0.048	Hashimoto (1990)
Mg_2SiO_4 (s)[b]	1873–2163	0.09–0.16	Hashimoto (1990)
Mg_2SiO_4 (l)[b]	2163–2323	0.20–0.21	Hashimoto (1990)

[a] Burns (1966) reported the melting point of corundum as 2310 K.
[b] Hashimoto (1990) reported the melting point of forsterite (Mg_2SiO_4) as 2163 K. The α_s values for Mg_2SiO_4 (s, l) are for Mg (g) and SiO (g) and are taken as equal for each.

The data of most interest are probably those for solid and liquid silica and for solid and liquid forsterite. These show vaporization coefficients for SiO (g) of ~ 0.04 in the 2173–2373 K range over liquid silica, to ~ 0.2 for SiO vaporized from Mg_2SiO_4 (liquid) in the same temperature range. If these vaporization coefficients are assumed to be valid for basaltic and komatiite lavas, the equilibrium partial vapor pressures of SiO may be about 5–25 times higher than the actual pressure. It remains to be seen whether or not the actual vaporization coefficients for SiO and other species vaporized from lavas are this much lower than unity, but the data in Table 10 indicate that the equilibrium partial pressures could be regarded as upper limits. However, SiO column densities above the tholeiitic and komatiitic lavas are still larger than those observed in space, even if $\alpha_s \sim 0.2$ for SiO, as reported for Mg_2SiO_4 liquid by Hashimoto (1990).

5. Summary

Based on our calculations and experimental studies, it appears inescapable that hot lavas on Io are vaporizing and losing Na, K, Si, Fe, and probably other elements of similar volatility. Some of these elements such as Na, K, and Fe are vaporized at least in part as monatomic gases, while other elements are vaporized in different molecular forms

(SiO, SiO_2, FeO). Reactions of these gases with sulfur and chlorine species in volcanic gases may lead to the formation of other unusual metallic vapors such as NaCl, KCl, $MgCl_2$, $FeCl_2$, and SiS. Fegley and Zolotov (2000) have already predicted formation of NaCl and KCl. However, the source(s) of the Na and K in ionian volcanic gases were not clear. It now appears that Na and K are present in volcanic gases because they are vaporized from the erupting lavas.

Observations of metallic vapors such as those listed above should be attempted during high temperature volcanic eruptions on Io, when these species are actively being produced. The published upper limits for metals in Io's atmosphere and the IPT are larger than the abundances predicted in our calculations, and thus do not rule out detection of the species which we predict to be present. In the case of magnesium, no upper limits for its abundance in Io's atmosphere exist. We particularly recommend searching for SiO, which is the most widespread Si-bearing molecule in space. The predicted SiO column densities above high temperature lavas on Io (e.g., tholeiite basalt, alkali basalt, and komatiite) are larger than the SiO column densities observed in other astronomical settings. We also note that the Na/K ratio of 10 ± 3 in Io's atmosphere (Brown, 2001) can be produced by fractional vaporization of the vapor generated by almost any lava we have modeled. The one cautionary note that should be kept in mind is that our predictions are for the equilibrium abundances of SiO and other gases. If the vaporization of lavas on Io is kinetically inhibited, as often observed during vaporization of solids into vacuo (Langmuir vaporization), then our predicted abundances are upper limits. It is unknown whether or not vaporization of an actively erupting lava will be kinetically inhibited on Io. However, SiO should still be observable even if kinetic effects inhibit its vaporization.

Finally, we echo our earlier recommendation for an Io volcanic probe mission to directly measure the pressure, temperature, and composition of volcanic gases from Pele or another hot spot on Io (Fegley and Zolotov, 2000). This is feasible using present technology and will vastly expand our understanding of the most volcanically active body in our Solar System.

Acknowledgments

This work is supported by Grants NAG5-11958 and NAG5-11037 from the NASA Planetary Atmospheres Program. We thank Nick Arndt, Brad Joliff, Jeff Kargel, Katharina Lodders, and Bob Nichols for helpful discussions.

Appendix A

This appendix lists all 109 rock compositions that were studied. The rock type, geographic location (or sample #, or meteorite name), and literature reference are listed. The total vapor pressure, Na/K atomic ratios in the melt and gas at 1900 K are also given in Table A.1.

Table A.1

		1900 K			
Rock type	Locality	$(Na/K)_{melt}$	$(Na/K)_{gas}$	Log P_{vap} (bars)	Reference
Felsic rocks					
Andesite		5.11	2720	−4.19	MacDonald (1972)
Andesite	Mount Hood	5.48	1226	−4.37	Murase and McBirney (1973)
Rhyolite	Newberry		12.5	−4.29	Murase and McBirney (1973)
Rhyolite		0.84	4.51	−4.70	MacDonald (1972)
Basalts					
Ocean island basalts					
Avg. alkali basalt	Auckland, NZ	4.45	5372	−3.73	Carmichael et al. (1974), Table 10-3-1
Basalt	Albemarle Island	14.71	14409	−4.05	Carmichael et al. (1974), Table 8-10-1
Tholeiitic basalt	Albemarle Island	8.48	8962	−4.05	Carmichael et al. (1974), Table 8-10-2
Olivine basalt	Ascenscion Island	6.82	6581	−4.04	Carmichael et al. (1974), Table 8-9-1
Olivine-poor basalt	Ascenscion Island	4.41	3511	−3.97	Carmichael et al. (1974), Table 8-9-2
Olivine basalt	Clarion Island	0.93	382	−3.91	Carmichael et al. (1974), Table 8-9-7
Alkali basalt	Fernando de Noronha	4.53	6426	−3.52	Carmichael et al. (1974), Table 8-4-6
Nepheline basanite	Fernando de Noronha	4.34	5592	−3.62	Carmichael et al. (1974), Table 8-4-7
Nephelinite (ankaratrite)	Fernando de Noronha	6.57	9295	−3.45	Carmichael et al. (1974), Table 8-4-5
Olivine basalt (1st episode)	Fuerteventura	7.48	9087	−3.85	Carmichael et al. (1974), Table 8-11-3
Olivine basalt	Gough Island	2.58	17732	−4.01	Carmichael et al. (1974), Table 8-8-5
Olivine basalt	Guadalupe Island	4.71	2650	−3.92	Carmichael et al. (1974), Table 8-9-8
Basalt, Hamakua series	Mauna Kea, HI	4.26	4901	−3.98	Carmichael et al. (1974), Table 8-13-4
Basalt	Hualalai, HI	5.22	6259	−3.94	Carmichael et al. (1974), Table 8-13-5
Basalt	Kilauea, HI	4.88	3944	−4.45	Carmichael et al. (1974), Table 8-13-3
Basalt, Waianae series	Oahu	11.98	9697	−4.34	Carmichael et al. (1974), Table 8-13-2
Picrite basalt	Kilauea, HI	5.99	5224	−4.03	Carmichael et al. (1974), Table 8-13-1
Historic flow of 1730–1736	Lanzarote	5.09	4521	−4.04	Carmichael et al. (1974), Table 8-11-6
Olivine basalt (1st episode)	Lanzarote	4.15	5791	−3.64	Carmichael et al. (1974), Table 8-11-1

Table A.1 (*Continued*)

Rock type	Locality	1900 K $(Na/K)_{melt}$	$(Na/K)_{gas}$	Log P_{vap} (bars)	Reference
Olivine basalt, last quaternary episode	Lanzarote	5.21	5600	−3.83	Carmichael et al. (1974), Table 8-11-5
Olivine basalt	Mauritius Island	17.62	21523	−3.90	Carmichael et al. (1974), Table 8-7-5
Olivine tholeiite	Roca Paciencia, Principe	2.71	2862	−4.10	Carmichael et al. (1974), Table 8-6-4
Alkali basalt	Roca Sundy, Principe	2.95	4703	−3.81	Carmichael et al. (1974), Table 8-6-2
Pyroxene–olivine basalt	Tenerife, lower Las Canadas series	3.62	4227	−3.56	Carmichael et al. (1974), Table 8-12-1
Basalt	St. Helena	3.82	3548	−3.90	Carmichael et al. (1974), Table 8-7-1
Ankaramite	Tahiti	2.05	3009	−3.88	Carmichael et al. (1974), Table 8-5-2
Basanite	Tahiti	2.99	2976	−3.74	Carmichael et al. (1974), Table 8-5-1
Olivine–augite basalt	Tahiti	3.33	4747	−3.91	Carmichael et al. (1974), Table 8-5-3
Tahitite	Tahiti	2.92	799	−3.54	Carmichael et al. (1974), Table 8-5-4
Nephelinite	Trinidade	7.31	10596	−3.35	Carmichael et al. (1974), Table 8-4-2
Nephelinite (ankaratrite)	Trinidade	3.11	3414	−3.43	Carmichael et al. (1974), Table 8-4-1
Sanidine nephelinite	Trinidade	2.70	1438	−3.43	Carmichael et al. (1974), Table 8-4-3
Alkali basalt	Tristan de Cunha	2.06	2757	−3.78	Carmichael et al. (1974), Table 8-8-1
Mid-ocean ridge basalts					
Oceanic tholeiite	mid-Atlantic ridge	32.68	34048	−4.08	Carmichael et al. (1974), Table 8-1-1
Oceanic tholeiite	mid-Atlantic ridge	20.64	24103	−4.08	Carmichael et al. (1974), Table 8-1-3
Basalt	mid-Atlantic ridge	7.23	8872	−4.00	Carmichael et al. (1974), Table 8-1-8
Basalt	mid-Atlantic ridge	7.97	9440	−4.11	Carmichael et al. (1974), Table 8-1-6
Basalt	mid-Atlantic ridge	27.25	31959	−4.05	Carmichael et al. (1974), Table 8-1-7
Oceanic tholeiite	mid-Atlantic ridge	20.99	24096	−4.03	Carmichael et al. (1974), Table 8-1-5
NMORB		46.16	54463	−4.08	Wilson (1989)
Continental tholeiites					
Avg. late Yakima–Ellenburg basalt	Columbia River Plateau	3.04	1657	−4.21	Carmichael et al. (1974), Table 9-1-6
Avg. Yakima basalt	Columbia River Plateau	3.04	1442	−4.26	Carmichael et al. (1974), Table 9-1-4
Basalt, base	Lesotho, Karroo basin, South Africa	5.52	4726	−4.26	Carmichael et al. (1974), Table 9-2-2
Basalt, top	Lesotho, Karroo basin, South Africa	4.56	3427	−4.24	Carmichael et al. (1974), Table 9-2-3
Olivine-enriched basalt	Lesotho, Karroo basin, South Africa	4.77	3487	−4.19	Carmichael et al. (1974), Table 9-2-1
Avg. Picture Gorge basalt	Columbia River Plateau	8.21	7989	−4.13	Carmichael et al. (1974), Table 9-1-2
Tholeiite	Columbia River Plateau	6.24	4824	−4.11	Murase and McBirney (1973)
Alkaline mafic rocks					
Felsic nephelinite	Moroto, eastern Uganda	4.25	1655	−3.33	Carmichael et al. (1974), Table 10-2-2
Ijolite	Napak, eastern Uganda	1.86	4054	−3.19	Carmichael et al. (1974), Table 10-2,-4
Melilitite nephelinite	Napak, eastern Uganda	1.76	3227	−3.36	Carmichael et al. (1974), Table 10-2-3
Nephelinite syenite	Napak, eastern Uganda	0.88	5.30	−3.40	Carmichael et al. (1974), Table 10-2-5
Olivine nephelinite	Moroto, eastern Uganda	3.04	4621	−3.50	Carmichael et al. (1974), Table 10-2-1
Ultrapotassic mafic rocks					
Jumillite	Murcia, southern Spain	0.64	404	−3.82	Carmichael et al. (1974), Table 10-4-4
Kalsilite leucitite	Bunyaruguru, Toro–Ankole province, East Africa	0.32	195	−3.55	Carmichael et al. (1974), Table 10-4-2
Leucite nephelinite	Nyiragongo, Birunga province, East Africa	1.46	1318	−3.32	Carmichael et al. (1974), Table 10-4-3
Madupite	Leucite Hills, WY	0.16	6.22	−3.51	Carmichael et al. (1974), Table 10-4-9
Olivine melilitite	Katunga volcano, Toro–Ankole province, East Africa	0.49	387	−3.26	Carmichael et al. (1974), Table 10-4-1
Orendite	Leucite Hills, WY	0.16	0.43	−3.10	Carmichael et al. (1974), Table 10-4-8
Shonkinite	Shonkin Shag sheet, Montana	0.91	674	−3.65	Carmichael et al. (1974), Table 10-4-6
Wyomingtonite	Leucite Hills, WY	0.19	0.60	−3.13	Carmichael et al. (1974), Table 10-4-7
Ultramafic rocks					
Dunite		4.56	347	−3.66	MacDonald (1972)
Khatangite 1985-139	Meimecha–Kotuj, Siberia	3.87	4413	−3.27	Kogarko and Ryabchikov (2000)
Khatangite 1985-143	Meimecha–Kotuj, Siberia	1.22	852	−3.62	Kogarko and Ryabchikov (2000)
Khatangite 1985-65	Meimecha–Kotuj, Siberia	2.92	2135	−3.35	Kogarko and Ryabchikov (2000)
Khatangite 1985-94	Meimecha–Kotuj, Siberia	1.91	3048	−3.27	Kogarko and Ryabchikov (2000)
Komatiite 8243	Barberton, South Africa	7.77	5454	−4.16	Arndt (2002, personal communication to B. Fegley)
Komatiite	Barberton, South Africa	15.20	14784	−4.49	Williams et al. (1999)
Komatiitic basalt	Cape Smith	9.12	8292	−4.68	Williams et al. (1999)
Komatiite	Commondale	60.79	35174	−4.47	Williams et al. (1999)
Komatiite	Kambalda	30.40	22366	−4.01	Williams et al. (1999)
Komatiite M664	Munro	5.07	4325	−4.35	Arndt (2002, personal communication to B. Fegley)

Table A.1 (*Continued*)

Rock type	Locality	1900 K $(Na/K)_{melt}$	1900 K $(Na/K)_{gas}$	1900 K Log P_{vap} (bars)	Reference
Meimechite 125	Meimecha–Kotuj, Siberia	0.20	186	−4.25	Arndt et al. (1995)
Meimechite 1985-18	Meimecha–Kotuj, Siberia	No Na	No Na	−5.62	Kogarko and Ryabchikov (2000)
Meimechite 24-4	Meimecha–Kotuj, Siberia	0.03	23.6	−4.67	Arndt et al. (1995)
Meimechite 26-6	Meimecha–Kotuj, Siberia	0.06	32.5	−4.91	Arndt et al. (1995)
Meimechite 29-1	Meimecha–Kotuj, Siberia	0.39	503	−4.35	Arndt et al. (1995)
Meimechite 37-2	Meimecha–Kotuj, Siberia	0.22	151	−5.01	Arndt et al. (1995)
Meimechite 595B	Meimecha–Kotuj, Siberia	0.19	66.8	−4.99	Arndt et al. (1995)
Meimechite 8313	Meimecha–Kotuj, Siberia	2.79	3496	−4.01	Kogarko and Ryabchikov (2000)
Meimechite E-1	Meimecha–Kotuj, Siberia	No Na	No Na	−5.54	Kogarko and Ryabchikov (2000)
Meimechite Gkh-31	Meimecha–Kotuj, Siberia	0.49	287	−4.00	Kogarko and Ryabchikov (2000)
Meimechite Gkh-33	Meimecha–Kotuj, Siberia	1.52	867	−4.39	Kogarko and Ryabchikov (2000)
Peridotite		8.36	2127	−4.50	MacDonald (1972)
Picrite 178K	Meimecha–Kotuj, Siberia	4.00	3856	−3.25	Arndt et al. (1995)
Picrite 1985-25	Meimecha–Kotuj, Siberia	0.19	270	−4.16	Kogarko and Ryabchikov (2000)
Picrite 1985-29	Meimecha–Kotuj, Siberia	No Na	No Na	−5.67	Kogarko and Ryabchikov (2000)
Picrite 1985-43	Meimecha–Kotuj, Siberia	1.29	1547	−3.73	Kogarko and Ryabchikov (2000)
Picrite 46-5	Meimecha–Kotuj, Siberia	0.28	357	−4.00	Arndt et al. (1995)
Picrite 47-3	Meimecha–Kotuj, Siberia	0.56	666	−4.01	Arndt et al. (1995)
Picrite 599	Meimecha–Kotuj, Siberia	0.17	186	−4.25	Arndt et al. (1995)
Picrite 7865	Meimecha–Kotuj, Siberia	No Na	No Na	−5.58	Kogarko and Ryabchikov (2000)
Meteorites					
CI chondrite		14.89	94.8	6.55	Anders and Grevesse (1989)
Enstatite chondrite	Peña Blanca Spring	33.94	2538	−4.13	Lodders et al. (1993)
Juvinas	Eucrites	16.34	12706	−4.92	Kitts and Lodders (1998)
Stannern	Eucrites	10.26	8062	−4.83	Kitts and Lodders (1998)
Chassigny	SNC	5.07	501	−4.07	Lodders (1998)
LEW 88516	SNC	29.35	15034	−4.14	Lodders (1998)
Nahkla	SNC	5.38	10128	−4.11	Lodders (1998)
Zagami	SNC	13.35	14441	−4.20	Lodders (1998)
CAIs					
Type A	Allende	No K	No K	−3.79	MacPherson et al. (1988), Table 10.3.2, #3
Type B1	Allende	27.36	8587	−4.19	MacPherson et al. (1988), Table 10.3.2, #1
Type B2	Allende	37.99	120137	−4.00	MacPherson et al. (1988), Table 10.3.2, #2
Type C	Allende	34.96	106397	−4.70	Wark (1983)
MUM3	Murchison	No K	No K	−4.51	MacPherson et al. (1988), Table 10.3.2, #7
Other					
Lunar mare basalt	Apollo 12 sample 12002	6.08	5456	−4.78	Williams et al. (1999)

References

Alcock, C.B., Peleg, M., 1967. Vaporization kinetics of ceramic oxides at temperatures around 2000 °C. Trans. Brit. Ceram. Soc. 66, 217–232.

Anders, E., Grevesse, N., 1989. Abundances of the elements: meteoritic and solar. Geochim. Cosmochim. Acta 53, 197–214.

Arndt, N., Lehnert, K., Vasil'ev, Y., 1995. Meimechites: highly magnesian lithosphere-contaminated alkaline magmas from deep subcontinental mantle. Lithos 34, 41–59.

Baig, M.A., Connerade, J.P., 1979. Rydberg series in the vacuum ultraviolet absorption spectrum of silicon monoxide. J. Phys. B 12, 2309–2318.

Berman, R.G., 1983. A thermodynamic model for multicomponent melts, with application to the system CaO–MgO–Al_2O_3–SiO_2. PhD thesis. Univ. Br. Columbia.

Berman, R.G., Brown, T.H., 1984. A thermodynamic model for multicomponent melts, with application to the system CaO–Al_2O_3–SiO_2. Geochim. Cosmochim. Acta 48, 661–678.

Bouchez, A.H., Brown, M.E., Schneider, N.M., 2000. Eclipse spectroscopy of Io's atmosphere. Icarus 148, 316–319.

Brown, R.A., 1974. Optical line emission from Io. In: Woszczyk, A., Iwaniszewska, C. (Eds.), Exploration of the Solar System. Reidel, Hingham, MA, pp. 527–531.

Brown, M.E., 2001. Potassium in Europa's atmosphere. Icarus 151, 190–195.

Burns, R.P., 1966. Systematics of the evaporation coefficients Al_2O_3, Ga_2O_3, In_2O_3. J. Chem. Phys. 44, 3307–3319.

Carmichael, I.S.E., Turner, F.J., Verhoogen, J., 1974. Igneous Petrology. McGraw–Hill, New York.

Carr, M., 1986. Silicate volcanism on Io. J. Geophys. Res. 91, 3521–3532.

Centolanzi, F.J., Chapman, D.R., 1966. Vapor pressure of tektite glass and its bearing on tektite trajectories determined from aerodynamic analysis. J. Geophys. Res. 71, 1735–1749.

Chase, M.W., 1998. NIST-JANAF Thermochemical Tables, 4th edition, J. Phys. Chem. Ref. Data, Monogr., Vol. 9.

Chervonnyi, A.D., Piven, V.A., Kashireninov, O.E., Manelis, G.B., 1977. Mass-spectrometric investigations of gas-phase equilibria over Al_2O_3 at high temperatures. High Temp. Sci. 9, 99–108.

Davies, A.G., 1996. Io's volcanism: thermo-physical models of silicate lava compared with observations of thermal emission. Icarus 124, 45–61.

Davies, A.G., Keszthelyi, L.P., Williams, D.A., Phillips, C.B., McEwen, A.S., Lopes, R.M.C., Smythe, B., Kamp, L.W., Soderblom, L.A., Carlson, R.W., 2001. Thermal signature, eruption style, and eruption evolution at Pele and Pillan on Io. J. Geophys. Res. 106, 33079–33103.

DeMaria, G., Balducci, G., Guido, M., Piacente, V., 1971. Mass spectrometric investigation of the vaporization process of Apollo 12 lunar samples. Proc. Second Lunar Sci. Conf., Geochim. Cosmochim. Acta 2 (Suppl. 2), 1367–1380.

Drowart, J., DeMaria, G., Burns, R.P., Inghram, M.G., 1960. Thermodynamic study of Al_2O_3 using a mass spectrometer. J. Chem. Phys. 32, 1366–1372.

Eska, V., von Zahn, U., Plane, J.M.C., 1999. The terrestrial potassium layer (75–110 km) between 71°S and 54°N: observations and modeling. J. Geophys. Res. 104, 17173–17186.

Farber, M., Srivastava, R.D., Yu, O.M., 1972. Mass spectrometric determination of the thermodynamic properties of the vapour species from alumina. JCS Faraday Trans. I 68, 249–258.

Fegley Jr., B., Cameron, A.G.W., 1987. A vaporization model for iron/silicate fractionation in the Mercury protoplanet. Earth Planet. Sci. Lett. 82, 207–222.

Fegley Jr., B., Zolotov, M.Yu., 2000. Chemistry of sodium, potassium, and chlorine in volcanic gases on Io. Icarus 148, 193–210.

Fegley Jr., B., Schaefer, L., Kargel, J., 2003. Vapor pressure vapor composition, and fractional vaporization of high temperature lavas on Io. In: Proc. Lunar Planet. Sci. Conf. 34th. Abstract 1686.

Gast, P.W., Hubbard, N.J., 1970. Abundance of alkali metals, alkaline and rare earths, and strontium-87/strontium-86 ratios in lunar samples. Science 167, 485–487.

Geissler, P.E., McEwen, A.S., Ip, W., Belton, M.J.S., Johnson, T.V., Smyth, W.H., Ingersoll, A.P., 1999a. Galileo imaging of atmospheric emissions from Io. Science 285, 870–874.

Geissler, P., McEwen, A.S., Keszthelyi, L., Lopes-Gautier, R., Granahan, J., Simonelli, D.P., 1999b. Global color variations on Io. Icarus 140, 265–282.

Gibson Jr., E.K., Hubbard, N.J., 1972. Thermal volatilization studies on lunar samples. Proc. Third Lunar Sci. Conf., Geochim. Cosmochim. Acta 2 (Suppl. 3), 2003–2014.

Gooding, J.L., Muenow, D.W., 1977. Experimental vaporization of the Holbrook chondrite. Meteoritics 12, 401–408.

Groesbeck, T.D., Phillips, T.G., Blake, G.A., 1994. The molecular emission-line spectrum of IRC + 10216 between 330 and 358 GHz. Astrophys. J. Suppl. 94, 147–162.

Grossman, L., Ebel, D.S., Simon, S.B., Davis, A.M., Richter, F.M., Parsad, N.M., 2000. Major element chemical and isotopic compositions of refractory inclusions in C3 chondrites: the separate roles of condensation and evaporation. Geochim. Cosmochim. Acta 64, 2879–2894.

Hapke, B., 1989. The surface of Io: a new model. Icarus 79, 56–74.

Hashimoto, A., 1983. Evaporation metamorphism in the early solar nebula—evaporation experiments on the melt FeO–MgO–SiO_2–CaO–Al_2O_3 and chemical fractionations of primitive materials. Geochem. J. 17, 111–145.

Hashimoto, A., 1990. Evaporation kinetics of forsterite and implications for the early solar nebula. Nature 347, 53–55.

Hastie, J.W., Bonnell, D.W., 1985. A predictive phase equilibrium model for multicomponent oxide mixtures: Part II. Oxides of Na–K–Ca–Mg–Al–Si. High Temp. Sci. 19, 275–306.

Hastie, J.W., Bonnell, D.W., 1986. A predictive thermodynamic model of oxide and halide glass phase equilibria. J. Non-Crystalline Solids 84, 151–158.

Hastie, J.W., Horton, W.S., Plante, E.R., Bonnell, D.W., 1982a. Thermodynamic models of alkali-metal vapor transport in silicate systems. High Temp.–High Press. 14, 669–679.

Hastie, J.W., Plante, E.R., Bonnell, D.W., 1982b. Alkali vapor transport in coal conversion and combustion systems. In: Gole, J.L., Stwalley, W.C. (Eds.), Metal Bonding and Interactions in High Temperature Systems. American Chemical Society, Washington, DC, pp. 543–600.

Hastie, J.W., Bonnell, D.W., Plante, E.R., Horton, W.S., 1984. Thermodynamic activity and vapor pressure models for silicate systems including coal slags. In: Ribeiro da Silva, M.A.V. (Ed.), Thermochemistry and Its Applications to Chemical and Biochemical Systems. Reidel, Dordrecht, pp. 235–251.

Hatchell, J., Fuller, G.A., Millar, T.J., 2001. SiO in G34.26. Outflows and shocks in a high mass star forming region. Astron. Astrophys. 372, 281–290.

Ho, P.H., Burns, R.P., 1980. A mass spectrometric study of the AlO_2 molecule. High Temp. Sci. 12, 31–39.

Kargel, J.S., Fegley, B., 2002. Thinking outside the tetrahedron: ceramic volcanism and other frightening thoughts. In: Workshop on Thermally Extreme Volcanism on Io, Flagstaff, AZ.

Kargel, J.S., Fegley Jr., B., Schaefer, L., 2003a. Ceramic volcanism on refractory worlds: the cases of Io chondritic CAIs. In: Proc. Lunar Planet. Sci. Conf. 34th. Abstract 1964.

Kargel, J.S., 23 colleagues, 2003b. Extreme volcanism on Io: latest insights at the end of the *Galileo* era. EOS 84, 313–318.

Keszthelyi, L., McEwen, A.S., 1997a. Magmatic differentiation of Io. Icarus 130, 437–448.

Keszthelyi, L., McEwen, A.S., 1997b. Thermal models for basaltic volcanism on Io. Geophys. Res. Lett. 24, 2463–2466.

Kitts, K., Lodders, K., 1998. Survey and evaluation of eucrite bulk compositions. Meteor. Planet. Sci. 33, A197–A213.

Kogarko, L.N., Ryabchikov, I.D., 2000. Geochemical evidence for meimechite magma generation in the subcontinental lithosphere of Polar Siberia. J. Asian Earth Sci. 18, 195–203.

Krieger, F.J., 1966. The thermodynamics of the alumina/aluminum–oxygen vapor system. United States Air Force Project Rand RM-5042-PR. pp. 1–29.

Krönert, W., Boehm, A., 1972. Messungen des Dampfdruckes bei freier Verdampfung an Aluminiumoxid und Magnesiumoxid. Glas-Email-Keramo-Technik 9, 319–323.

Lellouch, E., Paubert, G., Moses, J.I., Schneider, N.M., Strobel, D.F., 2003. Volcanically emitted sodium chloride as a source for Io's neutral clouds and plasma torus. Nature 421, 45–47.

Le Picard, S.D., Canosa, A., Pineau des Forets, G., Rebrion-Rowe, C., Rowe, B.R., 2001. The $Si(^3P_J) + O_2$ reaction: a fast source of SiO at very low temperature; CRESU measurements and interstellar consequences. Astron. Astrophys. 372, 1064–1070.

Liu, S.-H., Fruehan, R.J., Morales, A., Ozturk, B., 2001. Measurement of FeO activity and solubility of MgO in smelting slags. Metall. Mater. Trans. B 32, 2001–2031.

Lodders, K., 1994. Retention of alkali elements during planetary accretion and differentiation. Meteoritics 29, 492–493.

Lodders, K., 1998. A survey of shergottite, nakhlite and chassigny meteorites whole-rock compositions. Meteor. Planet. Sci. 33, A183–A190.

Lodders, K., 2003. Solar System abundances and condensation temperatures of the elements. Astrophys. J. 591, 1220–1247.

Lodders, K., Palme, H., Wlotzka, F., 1993. Trace elements in mineral separates of the Peña Blanca Spring aubrite: implications for the evolution of the aubrite parent body. Meteoritics 28, 538–551.

Longhi, J., 1987. On the connection between mare basalts and picritic volcanic glasses. J. Geophys. Res. 92, E349–E360.

Longhi, J., 1991. Comparative liquidus equilibria of hypersthene-normative basalts at low pressure. Amer. Mineral. 76, 785–800.

Longhi, J., Pan, V., 1989. The parental magmas of the SNC meteorites. In: Proc. Lunar Planet. Sci. Conf. 19th, pp. 451–464.

Lopes-Gautier, R., Davies, A.G., Carlson, R., Smythe, W., Kamp, L., Soderblom, L., Leader, F.E., Mehlman, R., the Galileo NIMS Team, 1997. Hot spots on Io: initial results from Galileo's near infrared mapping spectrometer. Geophys. Res. Lett. 24, 2439–2442.

Lopes, R.M.C., 14 colleagues, 2001. Io in the near infrared: near-infrared mapping spectrometer (NIMS) results from the Galileo flybys in 1999 and 2000. J. Geophys. Res. 106, 33053–33078.

Lucas, R., Liszt, H.S., 2000. SiO in diffuse, translucent and "spiral-arm" clouds. Astron. Astrophys. 355, 327–332.

MacDonald, G.A., 1972. Volcanoes. Prentice–Hall, Englewood Cliffs, NJ.

MacPherson, G.J., Wark, D.A., Armstrong, J.T., 1988. Primitive material surviving in chondrites: Refractory inclusions. In: Matthews, M.S., Kerridge, J.F. (Eds.), Meteorites and the Early Solar System Kerridge. Univ. of Arizona Press, Tucson, pp. 746–807.

Marchis, F., de Pater, I., Davies, A.G., Roe, H.G., Fusco, T., Le Mignant, D., Descamps, P., Macintosh, B.A., Prangé, R., 2002. High-resolution Keck Adaptive Optics imaging of violent volcanic activity on Io. Icarus 160, 124–131.

Markova, O.M., Yakovlev, O.I., Semenov, G.A., Belov, A.N., 1986. Evaporation of natural melts in a Knudsen chamber. Geokhimiya 11, 1559–1568.

Matveev, V.S., 1986. Absorptivity of the $X^1\Sigma$–$A^1\Sigma$ and $X^1\Sigma$–$E^1\Sigma$ electron bands of high-temperature SiO vapor. J. Appl. Spectros. 45 (2), 183–188.

Matson, D.L., Blaney, D.L., Johnson, T.V., Veeder, G.J., Davies, A.G., 1998. Io the early Earth. In: Proc. Lunar Planet. Sci. Conf. 29th. Abstract 1650.

McEwen, A.S., 14 colleagues, 1998. High-temperature silicate volcanism on Jupiter's moon Io. Science 281, 87–90.

McNeil, W.J., Lai, S.T., Murad, E., 1998a. Differential ablation of cosmic dust and implications for the relative abundances of atmospheric metals. J. Geophys. Res. 103, 10899–10911.

McNeil, W.J., Lai, S.T., Murad, E., 1998b. Models of thermospheric sodium, calcium and magnesium at the magnetic equator. Adv. Space Res. 21, 863–866.

McNeil, W.J., Murad, E., Plane, J.M.C., 2002. Models of meteoric metals in the atmosphere. In: Murad, E., Williams, I.P. (Eds.), Meteors in the Earth's Atmosphere. Cambridge Univ. Press, Cambridge, UK, pp. 265–287.

Minh, Y.C., Irvine, W.M., Friberg, P., 1992. Molecular abundances in the Sagittarius A molecular cloud. Astron. Astrophys. 258, 489–494.

Mittlefehldt, D.W., 1987. Volatile degassing of basaltic achondrite parent bodies: evidence from alkali elements and phosphorus. Geochim. Cosmochim. Acta 51, 267–278.

Morabito, L.A., Synnott, S.P., Kupferman, P.N., Collins, S.A., 1979. Discovery of currently active extraterrestrial volcanism. Science 204, 972.

Moses, J.I., Zolotov, M.Yu., Fegley Jr., B., 2002a. Photochemistry of a volcanically driven atmosphere on Io: sulfur and oxygen species from a Pele-type eruption. Icarus 156, 76–106.

Moses, J.I., Zolotov, M.Yu., Fegley Jr., B., 2002b. Alkali and chlorine photochemistry in a volcanically driven atmosphere on Io. Icarus 156, 107–135.

Murase, T., McBirney, A.R., 1973. Properties of some common Igneous rocks and their melts at high temperatures. Geol. Soc. Am. Bull. 84, 3563–3592.

Na, C.Y., Trafton, L.M., Barker, E.S., Stern, S.A., 1998. A search for new species in Io's extended atmosphere. Icarus 131, 449–453.

Nagai, S., Niwa, K., Shinmei, M., Yokokawa, T., 1973. Knudsen effusion study of silica. J. Chem. Soc. Faraday Trans. I 69, 1628–1634.

Nash, D.B., Carr, M.H., Gradie, J., Hunten, D.M., Yoder, C.F., 1986. Io. In: Burns, J.A., Matthews, M.S. (Eds.), Satellites. Univ. of Arizona Press, Tucson, p. 1021.

Naughton, J.J., Derby, J.V., Lewis, V.A., 1971. Vaporization from heated lunar samples and the investigation of lunar erosion by volatilized alkalis. Proc. Second Lunar Sci. Conf., Geochim. Cosmochim. Acta 1 (Suppl. 2), 449–457.

Nichols Jr., R.H., Grimley, R.T., Wasserburg, G.J., 1998. Measurement of gas-phase species during Langmuir evaporation of forsterite. Meteor. Planet. Sci. 33, A115–A116.

O'Hara, M.J., Biggar, G.M., Richardson, S.W., 1970. Experimental petrology of lunar materials: the nature of mascons, seas and the lunar interior. Science 167, 605–607.

Paule, R.C., 1976. Mass spectrometric studies of Al2O3 vaporization processes. High Temp. Sci. 8, 257–266.

Paule, R.G., Margrave, J.L., 1967. Free-evaporation and effusion techniques. In: Margrave, J.L. (Ed.), The Characterization of High-Temperature Vapors. Wiley, New York, pp. 130–151.

Pearl, J.C., Sinton, W.M., 1982. Hot spots of Io. In: Morrison, D. (Ed.), Satellites of Jupiter. Univ. of Arizona Press, Tucson, pp. 724–744.

Peleg, M., Alcock, C.B., 1974. The mechanism of vaporization and the morphological changes of single crystals of alumina and magnesia at high temperatures. High Temp. Sci. 6, 52–63.

Plante, E.R., 1979. Vapor pressure measurements of potassium over K_2O–SiO_2 solutions by a Knudsen Effusion Mass Spectrometric Method. In: Hastie, J.W. (Ed.), NBS Special Publication 561/1: Characterization of High Temperature Vapors and Gases. National Bureau of Standards, Washington, DC, pp. 265–281.

Podmoshenskii, I.V., Polozova, L.P., Chirkov, V.N., Yakovleva, A.V., 1968. Ultraviolet absorption of thin quartz layers heated to the boiling point. J. Appl. Spectros. 9 (1), 707–708.

Porter, R.F., Chupka, W.A., Inghram, M.G., 1955. Mass spectrometric study of gaseous species in the Si–SiO_2 system. J. Chem. Phys. 23, 216–217.

Radebaugh, J., McEwen, A.S., Milazzo, M.P., Keszthelyi, L.P., Davies, A.G., Turtle, E.P., Dawson, D.D., 2004. Observations and temperatures of Io's Pele Patera from *Cassini* and *Galileo* spacecraft images. Icarus. This issue.

Richter, F.M., Davis, A.M., Ebel, D.S., Hashimoto, A., 2002. Elemental and isotopic fractionation of Type B calcium-, aluminum-rich inclusions: experiments, theoretical considerations, and constraints on their thermal evolution. Geochim. Cosmochim. Acta 66, 521–540.

Ringwood, A.E., Essene, E., 1970. Petrogenesis of lunar basalts and the internal constitution and origin of the Moon. Science 167, 607–610.

Sagan, C., 1979. Sulphur flows on Io. Nature 280, 750–753.

Schaefer, L., Fegley Jr., B., 2002. Vaporization of high temperature magmas on Io. BAAS 34, 904. Abstract.

Shimaoka, T.K., Miyano, N., Baba, T., Yamamoto, K., Nakamura, N., 1994. Volatilization of alkali metals from the heated Murchison (CM2) meteorite. Proc. NIPR Symp. Antarct. Meteorites 7, 164–177.

Shornikov, S.I., Archakov, I.Yu., Shul'ts, M.M., 1998. Mass spectrometric study of vaporization and thermodynamic properties of silicon dioxide. I. Composition of the gas phase and partial vapor pressures of the molecular forms over silicon dioxide. Russ. J. Gen. Chem. 68 (8), 1171–1177.

Shornikov, S.I., Archakov, I.Yu., Shul'ts, M.M., 1999. Mass spectrometric study of vaporization and thermodynamic properties of silicon dioxide: II. Determination of partial vaporization coefficients of silicon dioxide. Russ. J. Gen. Chem. 69 (2), 187–196.

Shornikov, S.I., Archakov, I.Yu., Shul'ts, M.M., 2000. Mass spectrometric study of evaporation and thermodynamic properties of silica: III. Equilibrium reactions of molecules occurring in the gas phase over silica. Russ. J. Gen. Chem. 70, 360–370.

Smith, B.A., Shoemaker, E.M., Keiffer, S.W., Cook, A.F. II, 1979a. The role of SO_2 in volcanism on Io. Nature 280, 738–743.

Smith, B.A., 21 colleagues, 1979b. The Jupiter system through the eyes of Voyager 1. Science 204, 951–972.

Spencer, J.R., Schneider, N.M., 1996. Io on the eve of the Galileo mission. Annu. Rev. Planet. Sci. 24, 125–190.

Stansberry, J.A., Spencer, J.R., Howell, R.R., Dumas, C., Vakil, D., 1997. Violent silicate volcanism on Io in 1996. Geophys. Res. Lett. 24, 2455–2458.

Stolper, E., 1982. Crystallization sequences of calcium–aluminum-rich inclusions from Allende: an experimental study. Geochim. Cosmochim. Acta 46, 2159–2180.

Stolyarova, V.L., 2001. A mass spectrometric study of the thermodynamic properties of oxide melts. Glass Phys. Chem. 27 (1), 3–15.

Stolyarova, V.L., Semenov, G.A., 1994. Mass Spectrometric Study of the Vaporization of Oxide Systems. Wiley, New York.

Storey, W.C., 1973. Volatilization studies on a terrestrial basalt and their applicability to volatilization from the lunar surface. Nature 241, 154–157.

Trafton, L., 1975. Detection of a potassium cloud near Io. Nature 258, 790–792.

Tsuji, T., Ohnaka, K., Hinkle, K.H., Ridgway, S.T., 1994. High resolution infrared spectra of silicon monoxide and silicon isotopic abundances in cool luminous stars. Astron. Astrophys. 289, 469–491.

Veeder, G.J., Matson, D.L., Johnson, T.V., Blaney, D.L., Gougen, J.D., 1994. Io's heat flow from infrared radiometry: 1983–1993. J. Geophys. Res. 99, 17095–17162.

Von Zahn, U., Gerding, M., Hoffner, J., McNeil, W.J., Murad, E., 1999. Iron, calcium, and potassium atom densities in the trails of Leonids and other meteors: strong evidence for differential ablation. Meteor. Planet. Sci. 34, 1017–1027.

Von Zahn, U., Höffner, J., McNeil, W.J., 2002. Meteor trails as observed by lidar. In: Murad, E., Williams, I.P. (Eds.), Meteors in the Earth's Atmosphere. Cambridge Univ. Press, Cambridge, UK, pp. 149–189.

Vorypaev, G.G., 1981. Spectral absorption of a low-temperature quartz plasma. J. Appl. Spectros. 35 (6), 1297–1299.

Wang, J., Davis, A.M., Clayton, R.N., Mayeda, T.K., Hashimoto, A., 2001. Chemical and isotopic fractionation during the evaporation of the FeO–MgO–SiO_2–CaO–Al_2O_3–TiO_2 rare Earth element melt system. Geochim. Cosmochim. Acta 65, 479–494.

Wark, D., 1983. The Allende meteorite: information from Ca–Al-rich inclusions on the formation and early evolution of the Solar System. Thesis. University of Melbourne.

Williams, D.A., Wilson, A.H., Greeley, R., 1999. Komatiites from the Commondale Greenstone Belt, South Africa: a potential analog to ionian ultramafics? In: Proc. Lunar Planet. Sci. Conf. 30th. Abstract 1353.

Williams, D.A., Davies, A.G., Keszthelyi, L.P., Greeley, R., 2001. The summer 1997 eruption at Pillan Patera on Io: implications for ultrabasic lava flow emplacement. J. Geophys. Res. 106, 33105–33119.

Wilson, M., 1989. Igneous Petrogenesis. Unwin Hyman, London.

Wolff, E.G., Alcock, C.B., 1962. The volatilization of high-temperature materials in vacuo. Trans. Brit. Ceram. Soc. 61, 667–687.

Yu, Y., Hewins, R.H., O' D. Alexander, C.M., Wang, J., 2003. Experimental study of evaporation and isotopic mass fractionation of potassium in silicate melts. Geochim. Cosmochim. Acta 67, 773–786.

Zaitsev, A.I., Shelkova, N.E., Mogutnov, B.M., 2000. Thermodynamics of Na_2O–SiO_2 melts. Inorg. Mat. 36, 529–543.

Zolotov, M.Yu., Fegley Jr., B., 1999. Oxidation state of volcanic gases and the interior of Io. Icarus 141, 40–52.

Zolotov, M.Yu., Fegley Jr., B., 2001. Chemistry and vent pressure of very high-temperature gases emitted from Pele volcano on Io. In: Proc. Lunar Planet. Sci. Conf. 31st. Abstract 1474.

Zmbov, K.F., Ames, L.L., Margrave, J.L., 1973. A mass spectrometric study of the vapor species over silicon and silicon oxides. High Temp. Sci. 5, 235–240.